MAGNETOHYDRODYNAMICS AT HEAVY ION COLLISIONS

ERIC MARCUS

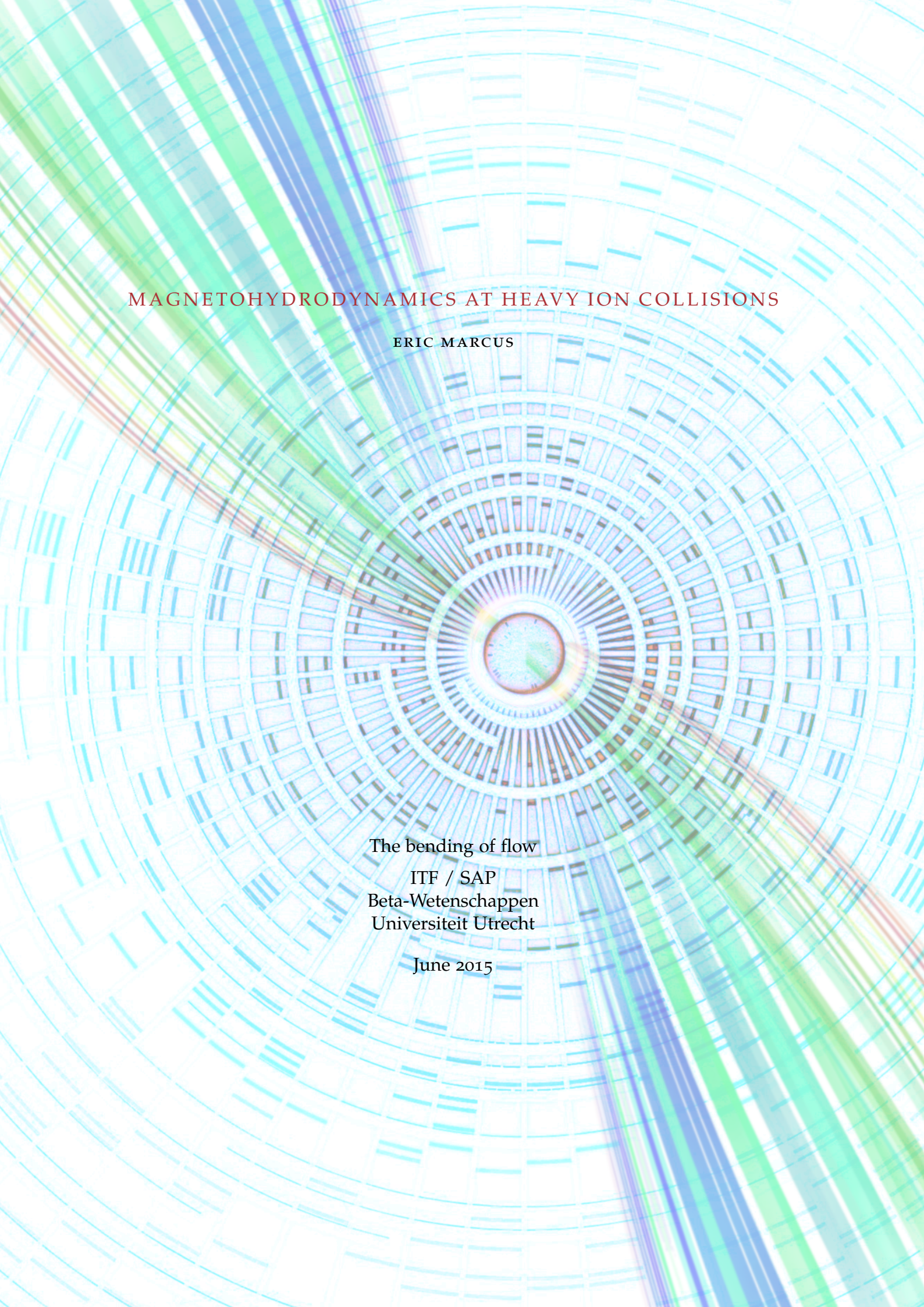

The bending of flow

ITF / SAP
Beta-Wetenschappen
Universiteit Utrecht

June 2015

SUPERVISORS:
Umut Gürsoy
Raimond Snellings
Jacopo Margutti

There is a theory which states that if ever anyone discovers exactly what the Universe is for and why it is here, it will instantly disappear and be replaced by something even more bizarre and inexplicable.
There is another theory which states that this has already happened.

— Douglas Adams, *The Restaurant at the End of the Universe*

ABSTRACT

Quantum Chromo Dynamics (QCD) predicts a phase transition from ordinary hadronic matter to a system with new degrees of freedom at temperatures accessible in laboratory. One of the main observations which lead to a paradigm change in the field was the observation of large anisotropic flow. An important ingredient in heavy ion collisions is the so-called impact parameter which defines the distance between the centers of colliding ions. In these collisions of charged ions also large electromagnetic fields should be present which affect the evolution of the formed QGP. These fields generate charged currents in the QGP which induce a Hall effect and a Faraday effect. We will derive explicit expressions for the electromagnetic fields.
The influence of these electromagnetic fields on the expansion of the QGP will be studied using relativistic viscous hydrodynamics. We will then show the influence of the electromagnetic fields on the directed, elliptic flow and triangular flow. We have obtained a solvable expression for any flow component v_n.

CONTENTS

ACRONYMS AND ABBREVIATIONS

QCD	Quantum Chromo Dynamics
QGP	Quark Gluon Plasma
HIC	Heavy Ion Collisions
LHC	Large Hadron Collider
RHIC	Relativistic Heavy Ion Collider
SO	Special Orthogonal group
ISO	Euclidean group
v_1	Directed flow
v_2	Elliptic flow
v_3	Triangular flow

Part I

THEORETICAL

In this section the details of the theory of magnetohydrodynamics will be explained. First there is a short introduction on electric and magnetic fields of moving particles in vacuum. After this we look at the fields when we introduce a constant conductivity in the medium. Having obtained the electromagnetic fields we can look at the hydrodynamics of the problem. Then we can study the influence of these fields on several flow coefficients. Our main focus will be the directed flow and elliptic flow but we have a solvable expression for v_n and show some results for triangular flow. We also present these flow harmonics integrated over a range of transverse momentum. The section is concluded by a discussion on the used parameters and their influence on the results.

1 INTRODUCTION

1.1 INTRODUCTION TO HEAVY ION COLLISIONS AND THE QGP

As predicted by Quantum Chromo Dynamics (QCD), there is a phase transition at high enough temperature to a Quark Gluon Plasma (QGP). This is a system with new degrees of freedom, and we are able to study it in the laboratory.

It consists of asymptotically free quarks and gluons

The QGP consists, as its name suggests, of quarks and gluons. These are fundamental building blocks of the world we know. It is hypothesized that this QGP existed for several microseconds after the big bang. It is also possible that the QGP might be present in the cores of neutron stars [23]. There are thus enough reasons to thoroughly study this phase of matter.

The laboratory where this is best studied is the Large Hadron Collider (LHC) at CERN Switzerland. At this collider there is a detector called ALICE (see also the experimental part of this thesis), where we collide heavy ions. In these collisions we try to reproduce this QGP.
An example of a collision is given in Fig 1. An important tool used in heavy ion collisions is the centrality. This states how central the collision was, so how 'perfect' the collision was. Something else noteworthy is that the originally approximate spherically shaped blobs of nucleons (heavy ions) become strongly contracted, due to Lorentz contraction. This happens because the ions travel near the speed of light.

1.2 ANISOTROPIC FLOW

One of the main observations which lead to a paradigm change was the observation of large elliptic flow. In addition to this elliptic flow there are different forms of anisotropic flow which provide information on the bulk properties of the matter and the initial geometry of the collision. The most prominent anisotropic flows we look at are the directed and the elliptic flow, noted by v_1 and v_2 respectively.
These flow components can be seen in a Fourier expansion of the differential azimuthal distributions of the particles, shown in Equation 1. We note that for later purposes, we are only interested in the small contribution to the anisotropies caused by the electromagnetic fields. This charge-dependent contribution is smaller than the total

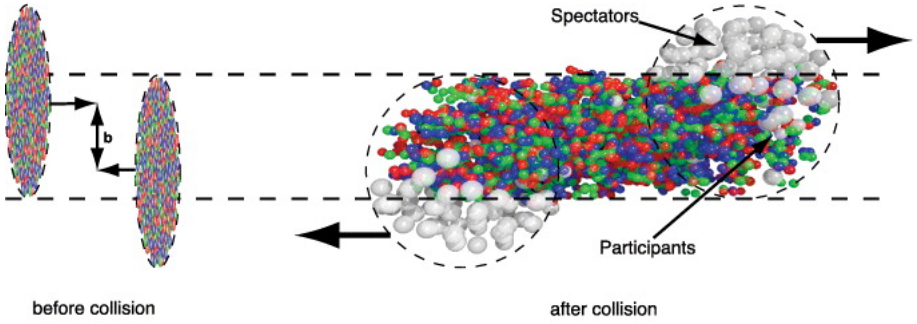

Figure 1: Here we show an example of a heavy ion collision. The left side shows the Lorentz-contracted blobs of protons before the collision. Important to note is that the $\vec{b}$ stands for the impact parameter and is the center to center distance at a collision. This defines the centrality of the collision. On the right hand side, the situation after the collision is shown. The participants are the particles that participate in the collision and the spectators do not participate. Figure from Ref. [23].

flow caused by the hydrodynamical response to the initial asymmetries.

$$E\frac{d^3N}{dp^3} = \frac{1}{2\pi}\frac{d^2N}{dp_T\,dY}\left(1 + 2\sum_{n=1}^{\infty} v_n\,\cos[n(\phi - \psi_{RP})]\right) \tag{1}$$

ψ_{RP} stands for the angle with the Reaction Plane defined by the collision. The flow components are defined as in Equation 2.

$$v_n = \langle \cos[n(\phi - \psi_{RP})]\rangle \tag{2}$$

Where the brackets define an average over all particles and all events (for a certain (p_T, Y) bin). As mentioned before, we will look mostly at the directed flow and the elliptic flow. The directed flow is the flow directed along transverse axes with respect to the beam axis. The elliptic flow is the elliptic expansion of the plasma in the transverse plane, as shown in Fig 2.

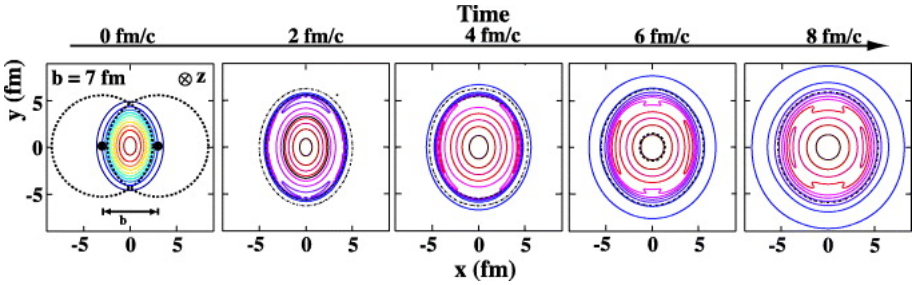

Figure 2: Shown here is the elliptic flow and its time dependence. One can see the characteristic elliptic shape of the expansion which defines elliptic flow. Note that the z-direction is the beam direction and here the x-axis is defined by the impact parameter. Figure from Ref. [23].

1.3 COORDINATE SYSTEM

In the field of particle physics there are some conventions for certain coordinates, some of which we will discuss here. Due to the detector layout it is useful to measure not ordinary momentum but transverse momentum. More importantly however, the transverse momentum is caused completely by the collision and therefore contains information on the collision.
It is the momentum in the transverse plane which is the orthogonal plane to the beam direction ($\hat{z}$), so this means it is the xy-plane.

The azimuthal angle ϕ is defined as the angle in the transverse plane.
Next there is pseudorapidity (η), which is a spatial coordinate describing the angle of the particle relative to the *beam axis* (not to confuse with ϕ).

$$\eta = -\ln\left(\tan\left(\frac{\theta}{2}\right)\right) \tag{3}$$

To get an idea how this translates to ordinary angles it is plotted in Fig 3.

Lastly there is the rapidity Y, which is not really a coordinate but an alternative way to describe speed.

$$Y = \tanh^{-1}\left(\frac{v_z}{c}\right) \tag{4}$$

So the rapidity maps the speed $-c < v < c$ to $-\infty < Y < \infty$. Note that in terms of rapidity the Lorentz factor $\gamma = 1/\sqrt{1-\frac{v^2}{c^2}}$ identifies with $\cosh(Y)$.

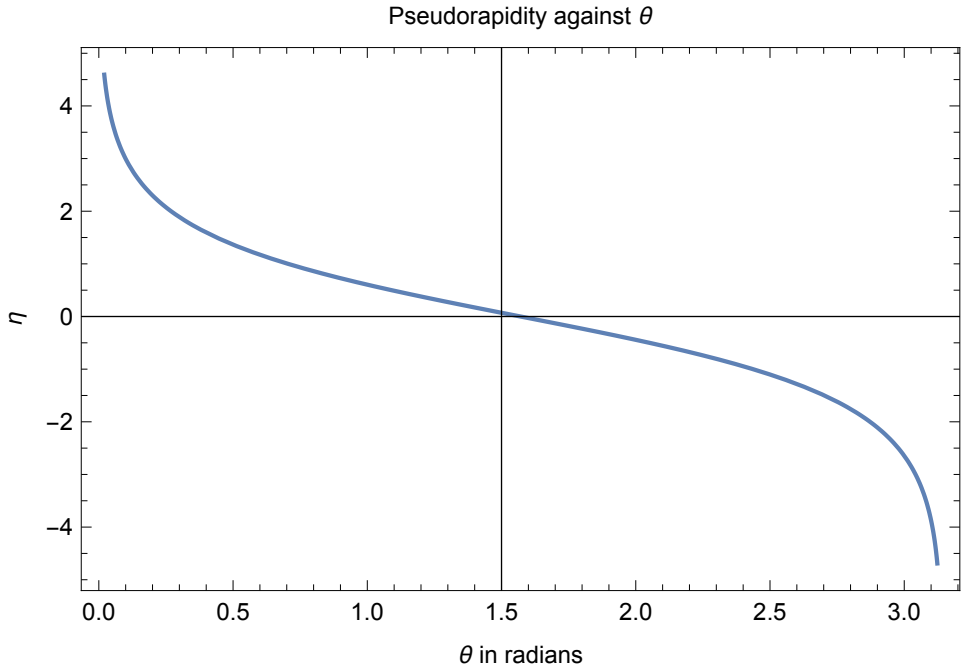

Figure 3: Pseudorapidity from Equation 3 plotted against the angle θ in radians.

1.4 THIS THESIS

In this thesis we shall be looking at heavy-ion collisions and in particular the present electromagnetic fields. The magnitude of these fields, at LHC, has been estimated to be of order $e|\vec{B}|/m_\pi^2 \approx 10 - 15$ [1].
We wish to obtain the influence of the electromagnetic fields on the expansion of the QGP and in particular the influence on the directed flow and elliptic flow. In practice we shall obtain just an order of magnitude estimate of these effects. We do this because this allows us to make several simplifying assumptions and get a mostly analytic calculation.

1.4.1 *Outline*

In this section a brief summary will be given of how this thesis is outlined. First there is a chapter on the magnetic field in vacuum, just to refresh some basic concepts. After this we shall incorporate the conductivity of the QGP to get eventually realistic expressions for the electromagnetic field present in heavy ion collisions. Note that we shall use a constant conductivity σ, which is not correct in reality, because it should depend on the temperature. See also Chapter 3.

To use these expressions, however, we shall first need a model to describe the expansion of the QGP without any of the electromagnetic effects, summarized by the four velocity u. We take for this the

analytic model found by Gubser [14].

Now, after this we want to get the velocity $\vec{v}$ caused by the electromagnetic field. To get this, however, we will need to boost to the local fluid rest frame where we have $\vec{u}' = 0$. In this *primed* frame (with $\vec{v}'$), all the components of $\vec{E}'$ and $\vec{B}'$ are non-zero. In order to get now the velocity $\vec{v}'$ we shall solve the equation of motion with the Lorentz force law and using stationary currents, see Equation 5. Note that this is a non-relativistic equation, which is only applicable in the case that $|\vec{v}| << |\vec{u}|$. We shall see later, Chapter 5, that this is actually a good assumption.

$$m \frac{d\vec{v}'}{dt} = q\vec{E}' + q\vec{v}' \times \vec{B}' - \mu m \vec{v}' = 0 \tag{5}$$

Where here the last term denotes the drag force on a fluid element with mass m on which the electromagnetic force is exerted, μ is the drag coefficient. The calculation of μm is not trivial and may be obtained from lattice QCD calculations. Instead we choose to use $N = 4$ supersymmetric Yang-Mills (SYM) theory. We do this to keep an analytic solution.
The drag force coefficient is currently only known precisely for heavy quarks in the $N = 4$ SYM theory, as derived in Ref. [24].

Consider reading the paper [24], as we state but one of many interesting results derived.

$$\mu m = \frac{1}{2} \pi \sqrt{\lambda} T^2 \tag{6}$$

Where $\lambda = g^2 N_c$, called the t' Hooft coupling. Here g is the gauge coupling and N_c the number of colors, see also [25][26]. We shall pick just as in [1], $\lambda = 6\pi$ and further assume μm to be a constant. We take $T = \frac{3}{2} T_c$, where $T_c \approx 170$ MeV, the crossover temperature to hadrons. Note that this is less serious simplification than the already mentioned constant conductivity σ.

Now, in this local fluid rest frame we shall assume that there are equal distributions of up and down (anti)quarks. At this point we ignore other quarks and thus also any chemical potential due to strangeness and baryon number for example. In the local fluid rest frame we look at the effects on up and down (anti)quarks with their respective charges.
So for example, for positively charged species the velocity would be $\vec{v} = (\vec{v}'_u + \vec{v}'_{\bar{d}})/2$. Note that because we assume equal distributions, the velocity for negative charged species is simply $-\vec{v}$.
Finally, having obtained our four velocity in the fluid rest frame we shall boost back to the center of mass frame and obtain $V^{\pm\mu}$, the total four velocity. This then incorporates the expansion as found by the hydrodynamic model and the effects due to the electromagnetic

field.
With this four-velocity we can get the spectra of particles (protons and pions in our case) and by using Equation 1 we can compute the different flow components.
The obtained results for directed and elliptic flow are shown in Chapter 5 and Chapter 6 respectively. In Chapter 7 we discuss the most important parameters and their influence on the electromagnetic fields and flow harmonics.

2

B-FIELD FOR A MOVING PARTICLE IN VACUUM

2.1 INTRODUCTION

In this thesis we will look at the most significant influences of the electromagnetic field: the induction of electric currents in the QGP. These currents have two origins:

- First there is an electromagnetic field due to the moving spectators. This can be seen from the fact that moving charges (here: spectators) generate (besides their usual electric field) a magnetic field. When the spectators move away from the QGP their electromagnetic field drops, and thus changes in time. From classical electrodynamics we know that a changing magnetic field will result in an electric field, the induced Faraday current.
- Second there is the Hall effect that is induced due to the Lorentz force $\vec{F} = q\vec{E} + q\vec{v} \times \vec{B}$. This force is thus perpendicular to the longitudinal speed and the B-field. The Hall effect occurs because charged particles of different sign are directed to opposite sides, which in turn generates another electric field.

Note that we don't have any boundaries at which charge can build up, so in a sense this is not the traditional Hall effect.

Note that in order to describe this properly we need to incorporate conductivity, which will happen in the next chapter. For now we shall start by considering particles in vacuum.
Important to realize is that the collision has an initial longitudinal velocity $\vec{u}$ perpendicular to the B-field (and therefore parallel to the beam direction). The magnetic fields and directions are shown in Fig 4.

2.2 COMPUTING THE FIELDS

We first consider a particle in vacuum which, in the laboratory frame, moves constantly in the z-direction. If we consider the rest frame of the particle there will be no B field (the particle is at rest) and we can write the E-field for particle α as follows:

$$\vec{E} = \frac{1}{4\pi\epsilon_0}\frac{q}{r^2}\hat{r} \quad = \quad \frac{1}{4\pi\epsilon_0}\frac{q}{\sqrt{x_0^2 + y_0^2 + z_0^2}}\hat{r} \tag{7}$$

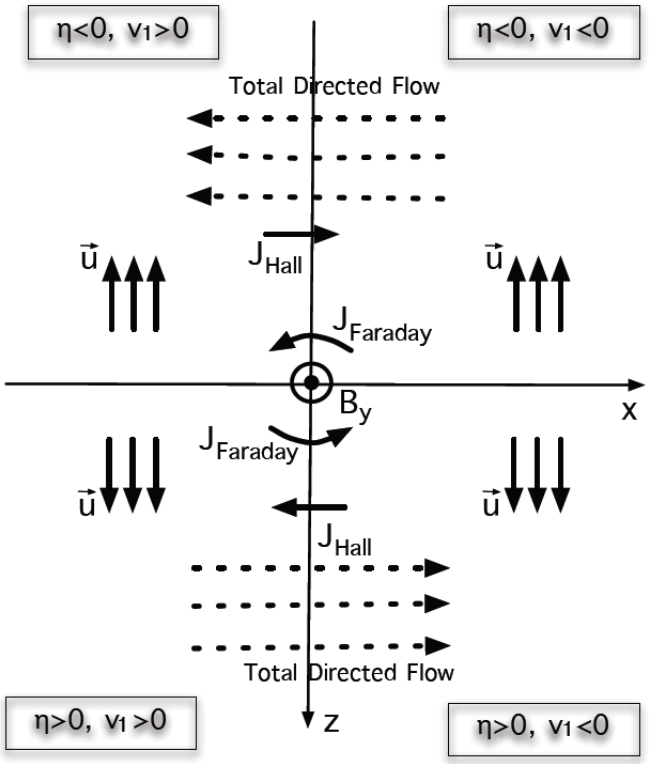

Figure 4: In the figure, η stands for the rapidity, v_1 for the directed flow, J_{Hall} for the induced Hall current, $J_{Faraday}$ for the induced Faraday current and B_y for the magnetic field in the y direction (perpendicular to beam direction). The collision happens in the z-direction, so we have $\vec{u}$ moving in the $\pm z$ direction. The dotted lines indicate the total directed flow in case that the Faraday effect outweighs the Hall effect. With these conventions we see that directed flow moving toward the negative x-axis is positive. Figure from *Ref. 1*

.

We now want to compute the electric and magnetic field in the laboratory frame. This is done by a Lorentz transformation in the $\hat{z}$ direction, given as:

$$F'^{\mu\nu} = \Lambda^{\mu}{}_{\alpha}\Lambda^{\nu}{}_{\beta}F^{\alpha\beta} \tag{8}$$

Where $F^{\mu\nu}$ is the electromagnetic field tensor and Λ is our Lorentz transformation. These are defined as:

$$F^{\mu\nu} = \begin{pmatrix} 0 & -E_1 & -E_2 & -E_3 \\ E_1 & 0 & -B_3 & B_2 \\ E_2 & B_3 & 0 & -B_1 \\ E_3 & -B_2 & B_1 & 0 \end{pmatrix} \quad \Lambda^{\mu}{}_{\nu} = \begin{pmatrix} \gamma & 0 & 0 & -\beta\gamma \\ 0 & 1 & 0 & 0 \\ 0 & 0 & 1 & 0 \\ -\beta\gamma & 0 & 0 & \gamma \end{pmatrix}$$

We can now calculate our transformed E and B fields as

$$E_1' = \gamma(E_1 - \beta B_2) \quad E_2' = \gamma(E_2 + \beta B_1) \quad E_3' = E_3 \tag{9}$$
$$B_1' = \gamma(B_1 + \beta E_2) \quad B_2' = \gamma(B_2 - \beta E_1) \quad B_3' = B_3 \tag{10}$$

In our original frame (the restframe) we had no B-field however, so we can disregard these. Furthermore we write our coordinates in the lab frame in terms of the vector $R_\alpha = r - r_\alpha(t)$ where r stands for the location where we calculate the magnetic field and $r_\alpha(t)$ is indicating the position of a particle α at time t. After some algebra we obtain the following expression for our E-field (where we have taken $c = 1$):

$$e\vec{E}_\alpha = \alpha_{em} \frac{(1-v_\alpha^2)\vec{R_\alpha}}{(1 - v_\alpha^2 \sin^2\theta)^{\frac{3}{2}}} \frac{1}{R_\alpha^3} \tag{11}$$

Where α_{em} indicates the electromagnetic coupling strength. We can rewrite this denominator as a cross product and then sum over all α to get:

$$e\vec{E}_{tot} = \sum_\alpha \frac{(1-v_\alpha^2)\vec{R_\alpha}}{R_\alpha^3(1 - (\vec{R_\alpha} \times \vec{v_\alpha})^2/R_\alpha^2)^{\frac{3}{2}}} \tag{12}$$

Now using our transformations in Equation 10 we can follow the same procedure for the B field or we can use $\vec{B} = (\vec{v}_\alpha \times \vec{E})$ and get:

$$e\vec{B}_{tot} = \sum_\alpha \frac{(1-v_\alpha^2)(\vec{v}_\alpha \times \vec{R_\alpha})}{R_\alpha^3(1 - (\vec{R_\alpha} \times \vec{v_\alpha})^2/R_\alpha^2)^{\frac{3}{2}}} \tag{13}$$

These two equations describe the electric and magnetic field caused by a collection of particles (for example two heavy ions). When calculating this we have however assumed that the particles travel on straight lines before and after scattering, also known as the eikonal approximation. At high energies this is a good approximation.
We now have calculated our magnetic field due to moving particles in vacuum. Note that these exact same fields can also be calculated using the Liénard-Wiechert potentials.

3

CONDUCTIVITY

3.1 INTRODUCTION

In the previous section the electromagnetic fields in vacuum were computed. In order to describe the electromagnetic field in the QGP, however, we need also include medium effects.
This strongly interacting medium is formed as early as 0.5 fm/c [2]. And even before this there is a strongly interacting medium in the form of a Glasma [3, 4]. So clearly we need to introduce conductivity in our equations to describe the electromagnetic fields properly.

It should be realized that the conductivity σ is actually temperature dependent as the plasma expands and changes. It is, however, convenient to take a conductivity that is constant because this allows us to get analytic results. Therefore we will first estimate a reasonable value for the conductivity and use this constant value to calculate the fields.

To obtain this reasonable value for σ, we look at recent lattice calculations [5-9]. The results of the calculations are usually shown as $C_{em}^{-1}\sigma/T$, where $C_{em}^{-1} = (\frac{4}{9} + \frac{1}{9} + \frac{1}{9})e^2 = 0.061$ (in three flavour QCD). At $T = 1.5T_c$ we observe that C_{em}^{-1} lies between 0.2 and 0.4 [5-9], where $T_c \approx 170$ MeV is the temperature of the crossover from a hadron gas to a QGP. Just as in [1] we set $\sigma = 0.023 fm^{-1}$ which corresponds to $C_{em}^{-1}\sigma/T = 0.3$ at $T = 1.5T_c$.

3.2 MAXWELL EQUATIONS

We will now formulate our Maxwell equations and include a conductivity σ in these equations. To model moving charge density we use Dirac delta functions. One for the $\hat{z}$ direction, in which the particle is moving, and one for the location in the transverse plane denoted with $\vec{x}_\perp$ and $\vec{x}'_\perp$. Where these vectors denote the location where we calculate the $\vec{B}$ and the location of the particle, respectively. We note that in total our $\vec{B}$ field is a function of the variables $\vec{x}_\perp$, $\vec{x}'_\perp$, z and t.

Besides this charge density we incorporate the conductivity as Ohm's law $J = \sigma\vec{E}$. We write our Maxwell equations as:

$$\vec{\nabla}\cdot\vec{B}=0 \qquad \vec{\nabla}\times\vec{E}=-\frac{\partial\vec{B}}{\partial t}$$
$$\vec{\nabla}\cdot\vec{E}=e\delta(z-vt)\delta(\vec{x}_\perp-\vec{x}'_\perp) \quad \vec{\nabla}\times\vec{B}=\frac{\partial\vec{E}}{\partial t}+\sigma\vec{E}+e\,v\,\hat{z}\delta(z-vt)\delta(\vec{x}_\perp-\vec{x}'_\perp) \tag{14}$$

We can write these equations to a second order equation for the $\vec{B}$ field by taking the cross product of the last equation for $\vec{B}$ again and get

$$\vec{\nabla}\times(\vec{\nabla}\times\vec{B})=\vec{\nabla}(\vec{\nabla}\cdot\vec{B})-\vec{\nabla}^2\vec{B} \tag{15}$$

We now fill in our obtained expressions from Equation 14 and after some rewriting we get our second order equation for the $\vec{B}$ field.

$$\vec{\nabla}^2\vec{B}-\frac{\partial^2\vec{B}}{\partial t^2}-\sigma\frac{\partial\vec{B}}{\partial t}=-e\,v\,\vec{\nabla}\times(\hat{z}\delta(z-vt)\delta(\vec{x}_\perp-\vec{x}'_\perp)) \tag{16}$$

3.3 SOLVING WITH GREEN'S FUNCTION

3.3.1 *Introduction*

To solve our found equation for the $\vec{B}$ field we shall make use of Green's function. In this section the basic idea behind this function is explained.
In mathematics and physics Green's function is used to solve linear differential equations, so we look at equations like:

$$Lu(x)=f(x) \tag{17}$$

Where L is a linear differential operator, and u(x) is the function we want to know. The definition of the Green's function is as follows:

$$LG(x,s)=\delta(x-s) \tag{18}$$

It can also be defined with a minus sign in front of the Dirac delta.

Note that if the kernel of L is non-trivial, then the Green's function is not unique. The kernel of a linear map $L : V \to W$ between two vector spaces V and W is defined as the set of all elements v of V for which $L(v)=0$. So $\ker(L)=\{v\in V \mid L(v)=0\}$.

To see why this Green's function is so useful we integrate Equation 18 along with function $f(s)$ with respect to s.

$$\int LG(x,s)f(s)ds = \int \delta(x-s)f(s)ds = f(x)$$

Now we use Equation 17 and compare it with above expression.

$$Lu(x) = \int LG(x,s)f(s)ds = L\left(\int G(x,s)f(s)ds\right)$$

We could perform the last step because the linear differential operator L only works on x. So we see now that we can get rid of the differential operator all together and thus solve for $u(x)$.

$$u(x) = \int G(x,s)f(s)ds \tag{19}$$

One last thing we will use is that in our case the operator L is translation invariant, thus has constant coefficients with respect to x. This means that Green's function can be taken to be a convolution operator so that $G(x,s) = G(x-s)$.

3.3.2 *Applied Green's function*

We shall now apply Equation 19 to our found Equation 16. Firstly we write for convenience $\vec{x}_\perp - \vec{x}'_\perp = \vec{b}$ and thus instead of $u(x)$ we have $\vec{B}(z,\vec{b},t)$ and we take our $f(s)$ to be

$$f(z',\vec{b}',t') = -e\nu\vec{\nabla}\times\left(\hat{z}\delta(z'-\nu t')\delta(\vec{b}')\right)$$

So we get in total as a solution for $\vec{B}$ the following expression.

$$\begin{aligned}&\vec{B}(z,\vec{b},t) = \\ &= \iiint d^2\vec{b}'\,dz'\,dt'\,G(z-z',\vec{b}-\vec{b}',t-t')\,e\nu\vec{\nabla}\times\left((\hat{z}\delta(z'-\nu t')\delta(\vec{b}')\right)\end{aligned} \tag{20}$$

And our Green's function must now satisfy our linear differential operator from Equation 16.

$$\vec{\nabla}^2\vec{G} - \frac{\partial^2\vec{G}}{\partial t^2} - \sigma\frac{\partial\vec{G}}{\partial t} = -\delta(z-z')\delta(\vec{b}-\vec{b}')\delta(t-t') \tag{21}$$

3.3.3 *Solving Green's function*

To solve the (non-trivial) above Green's function we will have to look at Fourier transforms of G. We do this because Fourier transforms of derivatives are very convenient to work with.

$$\mathcal{F}(f')(q) = iq\,\mathcal{F}(f)(q) \tag{22}$$

So now for our Green's function we have the following three Fourier transforms:

$$\mathcal{F}_z\ G(z,\vec{b},t,z',\vec{b}',t') = \int_{-\infty}^{\infty} G(k_z,\vec{b},t,z',\vec{b}',t')\,e^{ik_z z}\,dz \tag{23}$$

$$\mathcal{F}_{\vec{b}}\ G(z,\vec{b},t,z',\vec{b}',t') = \int_{-\infty}^{\infty} G(z,\vec{k}_\perp,t,z',\vec{b}',t')\,e^{i\vec{k}_\perp\cdot\vec{b}}d^2\vec{b} \tag{24}$$

$$\mathcal{F}_t\ G(z,\vec{b},t,z',\vec{b}',t') = \int_{-\infty}^{\infty} G(z,\vec{b},\omega,z',\vec{b}',t')\,e^{-i\omega t}\,dt \tag{25}$$

We use now that G_f denotes the Fourier transform of G. We can now write out the left-hand side of Equation 21 for the Fourier transform of G using the expression in Equation 22.

$$\vec{\nabla}^2\vec{G}_f - \frac{\partial^2\vec{G}_f}{\partial t^2} - \sigma\frac{\partial\vec{G}_f}{\partial t} = -(k_z^2+k_\perp^2)\,G_f + \omega^2 G_f + i\,\sigma\,\omega\,G_f \tag{26}$$

The next step is of course to also Fourier transform the right-hand side of Equation 21. In general we get for a spatial Fourier transform:

$$\mathcal{F}_x\left(\delta(x-x_0)\right) = \int_{\infty}^{\infty} e^{-ikx}\delta(x-x_0)dx = e^{-ikx_0} \tag{27}$$

Using this relation on all our Dirac delta's (including correct minus signs) we can write for Equation 26:

$$-(k_z^2+k_\perp^2)\,G_f + \omega^2 G_f + i\,\sigma\,\omega\,G_f = -\left(e^{-ik_z z'}e^{-i\vec{k}_\perp\cdot\vec{b}'}e^{i\omega t'}\right) \tag{28}$$

Which then finally leads to:

$$G_f(k_z,\vec{k}_\perp,\omega) = \frac{e^{-ik_z z'}e^{-i\vec{k}_\perp\cdot\vec{b}'}e^{i\omega t'}}{k_z^2+k_\perp^2-\omega^2-i\sigma\omega} \tag{29}$$

The next step is to do another Fourier transform (now the inverse). If we do this we can get our original Green's function back:

$$G(z-z',\vec{b}-\vec{b}',t-t') = \int_{-\infty}^{\infty}\frac{d^2k_\perp}{(2\pi)^2}e^{\vec{k}_\perp\cdot(\vec{b}-\vec{b}')} \tag{30}$$
$$\int_{-\infty}^{\infty}\frac{dk_z}{2\pi}e^{ik_z(z-z')}\int_{-\infty}^{\infty}\frac{d\omega}{2\pi}e^{-i\omega(t-t')}\frac{1}{k_z^2+k_\perp^2-\omega^2-i\sigma\omega}$$

We now want to plug this solution for our Green's function back into our equation for the $\vec{B}$ field, Equation 20. Before we do this we write the cross product in it's Fourier image so that

$$\vec{\nabla} \times \left((\hat{z}\delta(z' - vt')\delta(\vec{b}') \right) \rightarrow \delta(z' - vt')\delta(\vec{b}')\ i\vec{k} \times \hat{z} \tag{31}$$

Where $\vec{k} = k_z\hat{z} + \vec{k_\perp}$. It can be seen when we plug this all in to our Equation 20 that the delta functions make $\vec{b}' = 0$ and that $z' = vt'$. If we then use that

$$\int dt' e^{it'(\omega - k_z v)} = 2\pi\delta(\omega - k_z v)$$

So that we can now write our expression for $\vec{B}$ as:

$$\vec{B}(z, \vec{b}, t) = 2\pi e v \int \frac{d^2k_\perp}{(2\pi)^2} e^{i\vec{b}\cdot\vec{k}_\perp} \int \frac{dk_z}{2\pi} e^{ik_z z} \tag{32}$$
$$\int \frac{d\omega}{2\pi} e^{-i\omega t} \frac{(i\vec{k} \times \hat{z})\delta(\omega - k_z v)}{k_z^2 + k_\perp^2 - \omega^2 - i\sigma\omega}$$

At this point the y-component of the $\vec{B}$ is computed (it will turn out that this is the only f component). To do this we simply take the inproduct with $\hat{y}$.

$$(\vec{k_\perp} \times \hat{z}) \cdot \hat{y} = -k_\perp \cos(\phi) \tag{33}$$

Also completing the integral over k_z along with the Dirac delta leads to the following expression:

$$\vec{B}_y = e\ \hat{y} \int\int \frac{1}{(2\pi)^2} \frac{-ik_\perp \cos(\phi)}{(\omega/v)^2 + k_\perp^2 - \omega^2 - i\sigma\omega}\ e^{-ibk_\perp \cos(\phi)}\ e^{i\omega(\frac{z}{v} - t)} d^2k_\perp d\omega \tag{34}$$

Where now $d^2k_\perp = k_\perp dk_\perp d\phi$. We now use a few steps to rewrite Equation 34 in a more convenient form.

$$\int_0^{2\pi} -ik_\perp \cos(\phi)\ e^{-ibk_\perp \cos(\phi)} d\phi = \frac{d}{db} \int_0^{2\pi} e^{-ibk_\perp \cos(\phi)} d\phi$$
$$\int_0^{2\pi} e^{-iz\cos(\phi)} d\phi = 2\pi\ J_0(z)$$
$$\frac{d}{db}\ J_0(bk_\perp) = 2\pi\ k_\perp\ J_1(bk_\perp)$$
$$\alpha_{em} = \frac{e^2}{4\pi}$$

Where the J_0 and J_1 denote Bessel functions, and α_{em} is the electromagnetic coupling strength. When we apply all this we get the following expression.

$$e\vec{B}_y = \frac{\alpha_{em}}{\pi}\,\hat{y}\int_0^\infty dk_\perp \int_{-\infty}^{\infty} d\omega\, \frac{J_1(bk_\perp)\,k_\perp^2}{\frac{\omega^2}{v^2}+k_\perp^2-\omega^2-i\sigma\omega}\, e^{i\omega(\frac{z}{v}-t)} \quad (35)$$

This we will consider our endpoint of solving the Green's function and our starting point of solving the final expression of $\vec{B}$. To solve this integral we can first try to solve it with the approximation where $v = 1$ (note we set c=1). After this the integral will be solved for arbitrary v.

3.4 SOLVING THE B-FIELD

3.4.1 *B-field for* $v = 1$

In this scenario we obtain the following expression that we want to solve.

$$e\vec{B}_y = \frac{\alpha_{em}}{\pi}\,\hat{y}\int_0^\infty dk_\perp \int_{-\infty}^{\infty} d\omega\, \frac{J_1(bk_\perp)\,k_\perp^2}{k_\perp^2-i\sigma\omega}\, e^{i\omega(z-t)} \quad (36)$$

Our approach to solving this will be with the usage of complex analysis. In particular we make use of the Residue theorem. In summary this theorem states that:

$$\oint_\gamma f(z)\,dz = 2\pi\,i\sum \mathrm{Res}(f,a_k) \quad (37)$$

This states that the closed integral around curve γ of function $f(z)$ is equal to the residues (and some factor) of function f at poles a_k. So applying this to our case, we can now complete the contour for complex ω in the complex plane and see what poles we have. So looking at the integrand (for ω):

$$\frac{e^{i\omega(z-t)}}{k_\perp^2-i\omega\sigma} = \frac{e^{i\omega(z-t)}}{i\sigma(\frac{k_\perp^2}{i\sigma}-\omega)}$$

We notice that we have a pole at $\omega = \frac{k_\perp^2}{i\sigma}$ and that our residue at this point is

$$\frac{1}{i\sigma}e^{-\frac{k_\perp^2}{\sigma}(t-z)}$$

And thus we can now solve the integral over ω as:

$$\int \frac{e^{i\omega(z-t)}}{k_\perp^2 - i\omega\sigma} d\omega = \frac{2\pi}{\sigma} e^{-\frac{k_\perp^2}{\sigma}(t-z)}$$

Which leads to the next expression.

$$e\,\vec{B}_y = \frac{2\,\alpha_{em}}{\sigma}\,\hat{y}\int_0^\infty dk_\perp\, k_\perp^2\, J_1(bk_\perp)\, e^{-\frac{k_\perp^2}{\sigma}(t-z)} \tag{38}$$

Now we're almost there, we only have to solve the last integral. For this we use Gradshteyn Ryzhik [10] and as the final expression we get (which is the same result as in [2]):

$$e\vec{B}_y = \hat{y}\,\frac{\alpha_{em}\, b\, \sigma}{2(t-z)^2}\, e^{\frac{b^2\sigma}{4(t-z)}} \tag{39}$$

3.4.2 *B-field for $v \neq 1$*

This scenario becomes somewhat more complicated, but the same methods are used. Again we use the residue theorem. Our start situation is now:

$$e\vec{B}_y = \frac{\alpha_{em}}{\pi}\,\hat{y}\int_0^\infty dk_\perp \int_{-\infty}^\infty d\omega\, \frac{J_1(bk_\perp)\, k_\perp^2}{\frac{\omega^2}{v^2} + k_\perp^2 - \omega^2 - i\sigma\omega}\, e^{i\omega(\frac{z}{v}-t)} \tag{40}$$

We can see we have poles at:

$$\omega_\pm = \frac{i\,\sigma\gamma^2 v^2}{2}\left(1 \pm \left(1 + \frac{4\,k_\perp^2}{\sigma^2\gamma^2 v^2}\right)^{\frac{1}{2}}\right)$$

Where $\gamma = \frac{1}{\sqrt{1-v^2}}$. We now close the contour in the lower half of the complex plane (to remain in the light cone), and thus we pick up ω_-. Now using our residue theorem we complete the integral over ω and get the following expression for the integral.

$$I = \int_0^\infty dk_\perp \int_{-\infty}^\infty d\omega\, \frac{J_1(bk_\perp)\, k_\perp^2}{\frac{\omega^2}{v^2} + k_\perp^2 - \omega^2 - i\sigma\omega}\, e^{i\omega(\frac{z}{v}-t)} \tag{41}$$

$$I = 2\pi \int_0^\infty \frac{dk_\perp\, J_1(bk_\perp)\, k_\perp^2\, e^{-|\omega_-|(t-\frac{z}{v})}}{\sigma\left(1 + \frac{4k_\perp^2}{\sigma^2\gamma^2 v^2}\right)^{\frac{1}{2}}} \tag{42}$$

To continue the following coordinate transformation is done:

$$u = \left(1 + \frac{4k_\perp^2}{\sigma^2 \gamma^2 \nu^2}\right)^{\frac{1}{2}} \quad du = \frac{1}{u}\left(\frac{4k_\perp dk_\perp}{\sigma^2 \gamma^2 \nu^2}\right) \tag{43}$$

The above coordinate transformation leads to a rather lengthy expression, but it is the integral we are worried about. As it turns out we can solve this integral exact again, using [10].

$$I = \tag{44}$$
$$= \frac{2\pi\,(\gamma^2\ \sigma^2\ \nu^2)}{4}\ \frac{\gamma\,\nu}{2}\ e^{(t-\frac{z}{v})\ \frac{\sigma\,\gamma^2\,\nu^2}{2}}\ \int_1^\infty \sqrt{u^2-1} J_1(\beta\ \sqrt{u^2-1}) e^{-\alpha\,u} du =$$
$$= \frac{2\pi\,(\gamma^2\ \sigma^2\ \nu^2)}{4}\ \frac{\gamma\,\nu}{2}\ e^{(t-\frac{z}{v})\ \frac{\sigma\,\gamma^2\,\nu^2}{2}}\ \sqrt{\frac{2}{\pi}}\ \beta(\alpha^2+\beta^2)^{-\frac{3}{4}}\ K_{\frac{3}{2}}(\sqrt{\alpha^2+\beta^2}) \tag{45}$$

Where we have defined $\alpha = (t - \frac{z}{v})\ \frac{\sigma\,\gamma^2\,\nu^2}{2}$ and $\beta = \frac{b\,\sigma\,\gamma\,\nu}{2}$. Further we note that $K_{\frac{3}{2}}$ is a modified Bessel function and also has an exact form:

$$K_{\frac{3}{2}}(z) = \sqrt{\frac{2}{\pi}}\ e^{-z}\,(1+\frac{1}{z})$$

At this point we reintroduce $\vec{b} = (\vec{x}_\perp - \vec{x}'_\perp)$ and we shall also make another coordinate transformation defined as follows:

$$\begin{aligned} t &= \cosh(\eta)\ \tau \qquad & \tau &= \sqrt{t^2 - z^2} \\ z &= \sinh(\eta)\ \tau \qquad & \eta &= \operatorname{artanh}(\tfrac{z}{t}) \\ \nu &= \frac{\sinh(Y)}{\cosh(Y)} \qquad & Y &= \operatorname{artanh}(\beta) \end{aligned} \tag{46}$$

Where β follows from $z' = \beta t$ with z' the z location of a moving particle (note that we're looking at a particle that moves in positive z direction). Furthermore, η is the pseudorapidity and Y is the rapidity. In principle the B-field is already solved of course, but it remains to put it into a nicer form. We take that $x_\perp = |\vec{x}_\perp|$ which we can express as $\vec{x}_\perp = x_\perp\ \cos(\phi)$ with ϕ the azimuthal angle (the same applies for $\vec{x}'_\perp$). After doing quite some algebra with the above expression and coordinate transformation we reach the following final expression for our B-field:

$$e\vec{B}_y^+(\tau,\eta,x_\perp,\phi) = \alpha_{em}\ \hat{y}\ \sinh(Y)\,(x_\perp\ \cos(\phi) - x'_\perp\ \cos(\phi')) \times \frac{\left(\frac{\sigma\,|\sinh(Y)|}{2}\sqrt{\Delta}+1\right)}{\Delta^{\frac{3}{2}}}\ e^{\mathcal{A}} \tag{47}$$

The + represents the fact that it is a positively moving ($+\hat{z}$) particle. Here we have defined A and Δ as follows:

$$A = \frac{\sigma}{2}\left(\sinh(Y)\,\sinh(Y-\eta) - |\sinh(Y)|\,\sqrt{\Delta}\right)$$
$$\Delta = \tau^2\,\sinh^2(Y-\eta) + (x_\perp)^2 + (x'_\perp)^2 - 2\,x_\perp\,x'_\perp\,\cos(\phi-\phi')$$

We conclude this section by noting that the same procedure can be applied to find the x component of the E-field to get:

$$eE_x = e\,B_y\,\coth(Y-\eta) \tag{48}$$

3.5 INTEGRATION

We now have a complete picture of what one particle (located at $\vec{x}'_\perp$ and $z' = \beta\,t$) would contribute to the magnetic field, so to get the total magnetic field we will have to integrate over the locations of all particles. The spectator and participant contribution will be integrated separately.

To get the complete contribution in either case, we need to add up the fields created by particles moving in both + and − z direction. So the total B-field would look like $\vec{B}_{tot} = \vec{B}_s^+ + \vec{B}_s^- + \vec{B}_p^+ + \vec{B}_p^-$. Here $\vec{B}_s^+$ denotes the B field due to a spectator moving in the + direction (the $\vec{B}_p$ denote the participants). At this point we will also make the simplifying approximation that the protons in a nucleus are distributed evenly in a sphere with Radius R. We then place the centers of the spheres at $x = \pm\,\frac{b}{2}$, $y = 0$ and moving of course along the $\pm\hat{z}$ direction. For a quick overview see the sketch in Fig 5.

We can now project the probability distribution of the protons on transverse plane. The distribution is then given as:

$$\rho_\pm(x_\perp) = \frac{3}{2\pi R^3}\,\sqrt{R^2 - \left(x_\perp^2 \pm b\,x_\perp\,\cos(\phi) + \frac{b^2}{4}\right)} \tag{49}$$

In both the cases we integrate over the coordinates ϕ' and $x'_\perp$ and in the case of the participant we will have to incorporate the loss of rapidity due to collisions.

To get both the contribution from positively and negatively moving particles we need to add up $\vec{B}^+ + \vec{B}^-$ with respective ρ's. But we can also do this by changing the coordinates in our expression for just $\vec{B}+$ so then $e\,B_y = e\,B_y^+(\tau,\eta,x_\perp,\pi-\phi) + e\,B_y^+(\tau,-\eta,x_\perp,\phi)$ and we only need apply ρ_-, see also next section.
One last remark, we shall use (unless mentioned otherwise) use the values $R = 7$ fm and $b = 7$ fm.

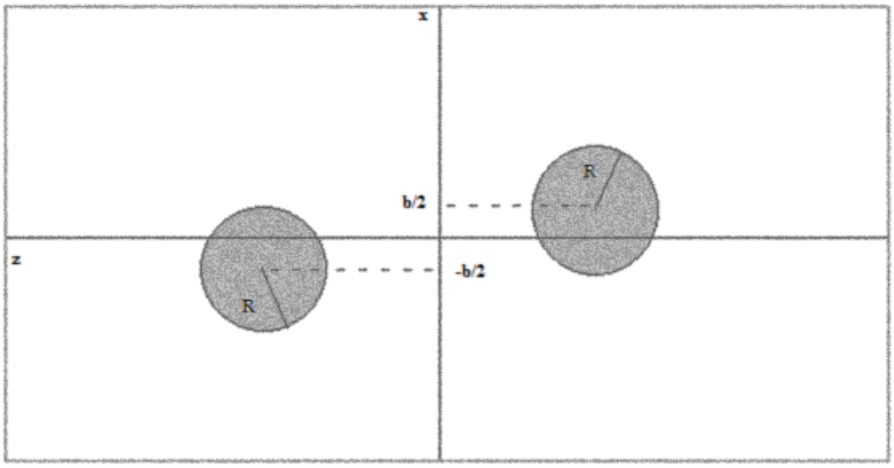

Figure 5: Here we see the two spheres with protons, they move toward each other. The spectators will be located in the parts where there will be either particles moving in the $+$ or $-\hat{z}$ direction, but not both.

3.5.1 *Spectators*

First we will have a look at the spectator contribution. Since these spectators don't participate in any collision, the rapidity they have before the collision is the same as after the collision. For this beam rapidity the we take the value $Y_0 \simeq 8.0$ (same value as in Ref[1]).
In order to get all the particles we need proper integration limits. For ϕ' these are $-\frac{\pi}{2}$ to $\frac{\pi}{2}$. For $x'_\perp$ we have to define the limits to get the crescent shaped locations where we find either positively or negatively moving particles but not both. It turns out that we can write these as:

$$x_{in/out}(\phi') = \mp\frac{b}{2}\cos(\phi) + \sqrt{R^2 - \frac{b^2}{4}\sin^2(\phi')} \tag{50}$$

Now with all these defined we can write our expressions for the electromagnetic fields due to the spectators.

$$\begin{aligned} e\,B_{y,s}(\tau,\eta,x_\perp,\phi) = -Z\int_{-\frac{\pi}{2}}^{\frac{\pi}{2}} d\phi' \int_{x_{in}(\phi')}^{x_{out}(\phi')} dx'_\perp\; x'_\perp \rho_-(x'_\perp) \\ \times\left(e\,B_y^+(\tau,\eta,x_\perp,\pi-\phi) + e\,B_y^+(\tau,-\eta,x_\perp,\phi)\right) \end{aligned} \tag{51}$$

$$\begin{aligned} e\,E_{x,s}(\tau,\eta,x_\perp,\phi) = Z\int_{-\frac{\pi}{2}}^{\frac{\pi}{2}} d\phi' \int_{x_{in}(\phi')}^{x_{out}(\phi')} dx'_\perp\; x'_\perp \rho_-(x'_\perp) \\ \times\left(-e\,E_x^+(\tau,\eta,x_\perp,\pi-\phi) + e\,E_x^+(\tau,-\eta,x_\perp,\phi)\right) \end{aligned} \tag{52}$$

Note the factor of Z in front of the integrals. This is clearly the charge of the used nucleus, which for LHC is Lead. So in our case we

have $Z = 82$.
This result for the magnetic field can be numerically integrated for example for $\eta = x_\perp = 0$, the result obtained is shown in Fig 6.

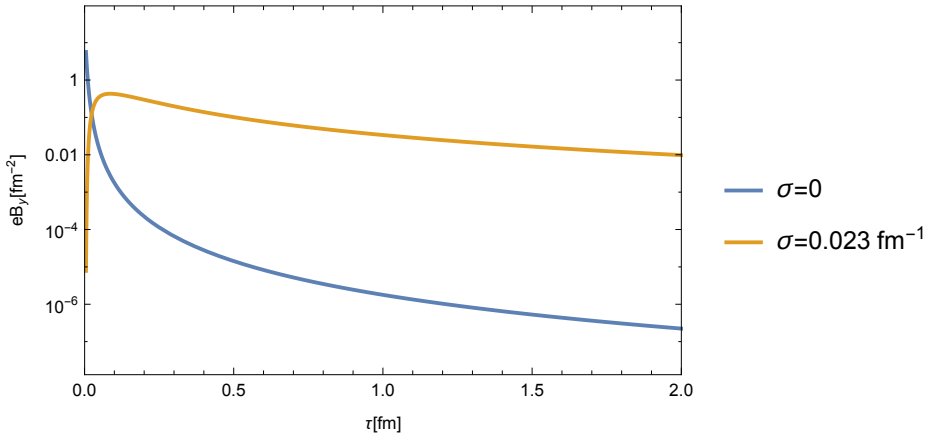

Figure 6: Here we see a comparison of the spectator-only B-fields with and without conductivity for $\eta = x_\perp = 0$. At very low τ the blue curve is a better approximation, but we will use the other curve instead since our calculation is not dependent on these very early times. Most important is however to notice that the conductivity delays the decrease of the magnetic field.

To have a look ahead we will look what the B-field will look like at the freeze-out surface. This surface will be defined and explored in the next chapter. So now it will be numerically integrated for η from -3 to 3, $x_\perp$ from 0 to approximately 18 (up to here we get a reasonable precise result) at $\tau = \tau_{freeze}(x_\perp)$, see Fig 7.

3.5.2 *Participants*

For the participants we need to also account for the change in rapidity Y. To do this we must have some distribution of Y after the collision for the protons. After the collision the $-\hat{z}$ moving protons must have the same distribution but then with $-Y$.
The distribution we use is an empirical distribution from [11,12]:

$$f(Y) = \frac{a}{2\sinh(a\,Y_0)}\, e^{a\,Y}, \qquad -Y_0 \leqslant Y \leqslant Y_0 \tag{53}$$

We now set the parameter $a \simeq \frac{1}{2}$. This has a deeper meaning in Regge theory, see [12], which we will not go into. It is however also consistent with experimental data on baryon stopping [12,13].
So, we can again define our expressions for the electromagnetic fields, but now for the participants:

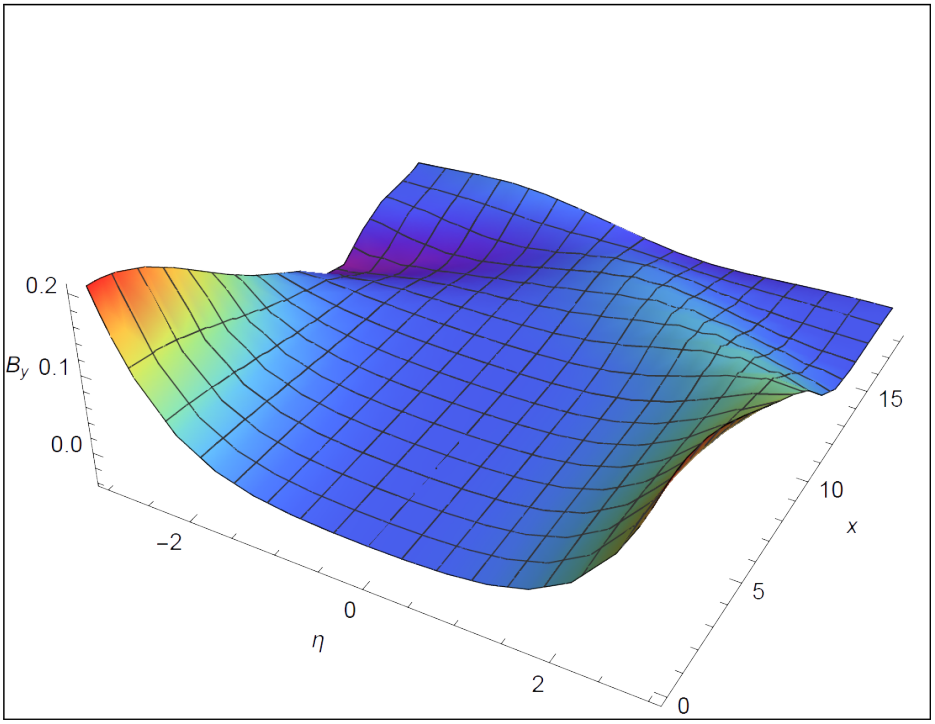

Figure 7: Plotted is the B-field produced by the spectators. It is shown for η from -3 to 3, $x_\perp$ from 0 to approximately 18 at $\tau = \tau_{freeze}(x_\perp)$. A detailed discussion into the freezeout surface is found in the chapter of Hydrodynamics.

$$e\,B_{y,p} = -Z \int_{-Y_0}^{Y_0} dY\, f(Y) \int_{-\frac{\pi}{2}}^{\frac{\pi}{2}} d\phi' \int_0^{x_{in}(\phi')} dx'_\perp\, x'_\perp \rho_-(x'_\perp) \qquad (54)$$
$$\times \left(e\,B_y^+(\tau, \eta, x_\perp, \pi - \phi) + e\,B_y^+(\tau, -\eta, x_\perp, \phi) \right)$$

$$e\,E_{x,p} = Z \int_{-Y_0}^{Y_0} dY\, f(Y) \int_{-\frac{\pi}{2}}^{\frac{\pi}{2}} d\phi' \int_0^{x_{in}(\phi')} dx'_\perp\, x'_\perp \rho_-(x'_\perp) \qquad (55)$$
$$\times \left(-e\,E_x^+(\tau, \eta, x_\perp, \pi - \phi) + e\,E_x^+(\tau, -\eta, x_\perp, \phi) \right)$$

We note now that the other components of the electromagnetic field are irrelevant because $B_z = 0$. And we can now also do a numerical integration of the total B-field which is shown in Fig 8.

3.5.3 *Participant and Spectator contribution*

The next question we would like to answer is the contribution from the participants and spectators to the total electromagnetic field. We can take the obtained expressions in the last two sections and numerically integrate them, after which we can compare their sizes.

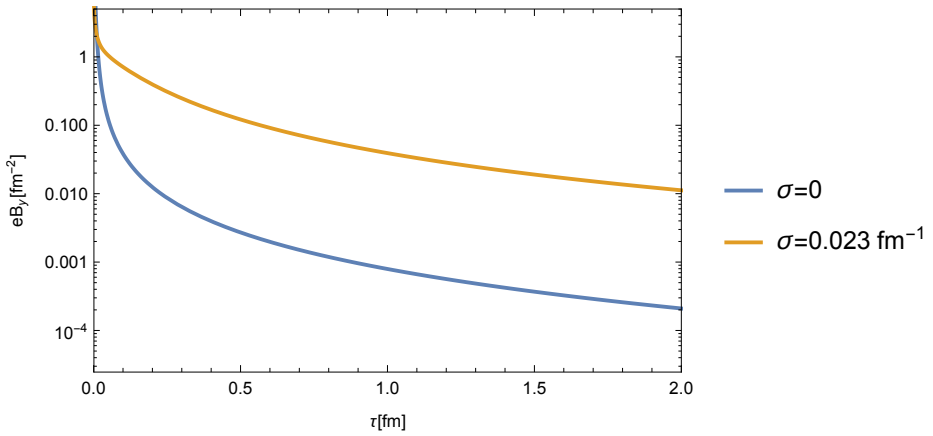

Figure 8: Here we plot the complete B-Field (spectator and participant) with and without conductivity, at $\eta = x_\perp = 0$. We can again see the delay in the decrease of the magnetic field due to the conductivity. Note that we do not need τ at very low values in our calculations later on.

A first comparison we could first make however is between Fig 6 and Fig 8. This already gives us the first hint that the participant contribution is not very large. In both plots we can see (not at very small τ) that there is a very minor difference between the two and therefore we expect the participants not to contribute that much.
It actually turns out that this intuition is correct and that the participants maximally contribute 10% to the total magnetic field and in general much less. We found this by numerical integration at appropriate ranges for τ, $x_\perp$, η and ϕ. So we can now conclude that for a qualitative analysis we can ignore the spectator contribution all together. For the final results of the directed flow, the contribution of the participants is hardly noticeable. The contribution to v_2, however, does seem to be important and we will not ignore the contribution there.

3.5.4 *Concluding*

In this section we have derived the full electromagnetic field due to the spectators and participants in a collision. We now want to apply these results to (a model of) the Quark Gluon Plasma and try to find out what the influence is of the EM-field.
To do this we shall first have to create such a model. In the upcoming section we shall first explore an analytic solution to approximate the flow of the QGP without any electromagnetic effects. After this we can apply our results of this section and determine the influence on the flow coefficients.

4

HYDRODYNAMICS

4.1 INTRODUCTION

At this point we want to get a reasonable, analytic, model to describe the expansion of the QGP (without any effects of the electromagnetic field). So this will give us a velocity u^μ that describes the change of the QGP.
After this we can apply the Cooper-Frye freeze-out procedure (see later). This procedure gives us hadron spectra from a certain hydrodynamic flow. Of course we want these spectra to reproduce spectra found experimentally at LHC (as good as possible, that is).

4.2 GUBSER'S MODEL

The analytic model we shall use is the one found by Gubser in 2010, see Ref [14]. For a full mathematical analysis and derivation of this model one should read the article [14] itself. Here we give a mere summary of the model and its predictions.
The model is a generalization of Bjorken flow where the medium has finite transverse size (which is true in our case) and expands both radially and transversely along the beam axis. When we assume that the equations of viscous hydrodynamics can be used, the flow described by Gubser's solution can be developed into an exact solution of the relativistic Navier-Stokes equations. The local four velocity (the one we are interested in) is completely determined by symmetry of a subgroup of the conformal group.
The conformal group in four dimensions is an extension of the Poincaré group $ISO(3,1)$ to $SO(4,2)$. Note that the Special Orthogonal group is a subgroup of the Orthogonal group with their determinant being 1. This SO group is also called the rotation group because in 2 and 3 dimensions its elements are merely the rotations around a point (2D) or a line (3D).

The Special Orthogonal group can also have a determinant of -1

After some research into the Lie Algebra of this conformal group (the generators), it becomes clear that Gubser's model aims to realize the flow of a fluid that conserves a subgroup $SO(3)_q \times SO(1,1) \times Z_2$ of the full four dimensional conformal group (so the extension to the Poincaré group). The q stands for the fact that that the $SO(3)$ depends on q [14], this is a parameter related to inverse length (so not charge). The Z_2 comes from the invariance under $z \to -z$ (or $\eta \to -\eta$).

Gubser finds that the only four velocity respecting the above symmetries is given as in Equation 56 and Equation 57.

$$u^\tau = \frac{1 + q^2\tau^2 + q^2 x_\perp^2}{2\,q\,\tau\sqrt{1+g^2}} \tag{56}$$

$$u^\perp = \frac{q\,x_\perp}{\sqrt{1+g^2}} \tag{57}$$

Where the variable g is given in Equation 58.

$$g = \frac{1 + q^2\,x_\perp^2 - q^2\,\tau^2}{2\,q\,\tau} \tag{58}$$

Gubser then goes on to solve the local temperature of the fluid under condition that we preserve the conformal invariance of the theory. This is equivalent to saying that

$$p = \frac{\epsilon}{3} \tag{59}$$

$$\eta = \epsilon^{\frac{3}{4}}\,H_0 \tag{60}$$

Where now ϵ stands for the energy density and H_0 is a dimensionless constant. Taking these conditions into consideration Gubser finds the following solution for the local fluid temperature:

$$T(g) = \frac{1}{\tau\,f_*^{1/4}}\left(\frac{\hat{T}_0}{(1+g^2)^{1/3}} + \frac{H_0\,g}{\sqrt{1+g^2}}\left[1 - (1+g^2)^{1/6}\;{}_2F_1\left(\frac{1}{2},\frac{1}{6};\frac{3}{2};-g^2\right)\right]\right) \tag{61}$$

Note that again, the parameter q is proportional to the inverse length and we will have to fix this constant to get a reasonable fit for our experimental spectra from LHC later on.
Furthermore, $\hat{T}_0$ is a constant from integration, f_* relates the energy density and local temperature as $\epsilon = f_* T^4$ and H_0 indicates the strength of the viscous corrections (see also Equation 59). It still remains to fix these constants to get a reasonable solution for our situation.

We shall follow Gubser in his choice for these constants, except for q and $\hat{T}_0$. So following Ref. [14] we use $f_* = 11$, which is a reasonable choice for the QGP at $T \approx 300$ MeV, see also [15]. Now, $H_0 = 0.33$ is chosen so that it corresponds to $\eta/s = 0.134$, see Equation 60. Note that η/s is the shear viscosity divided by the entropy density. This value of η/s follows from SU(3) gluodynamics, see [16]. It is slightly bigger than $\eta/s = 1/4\pi$, which had been proposed to correspond to the QGP in earlier publications [17] [18].

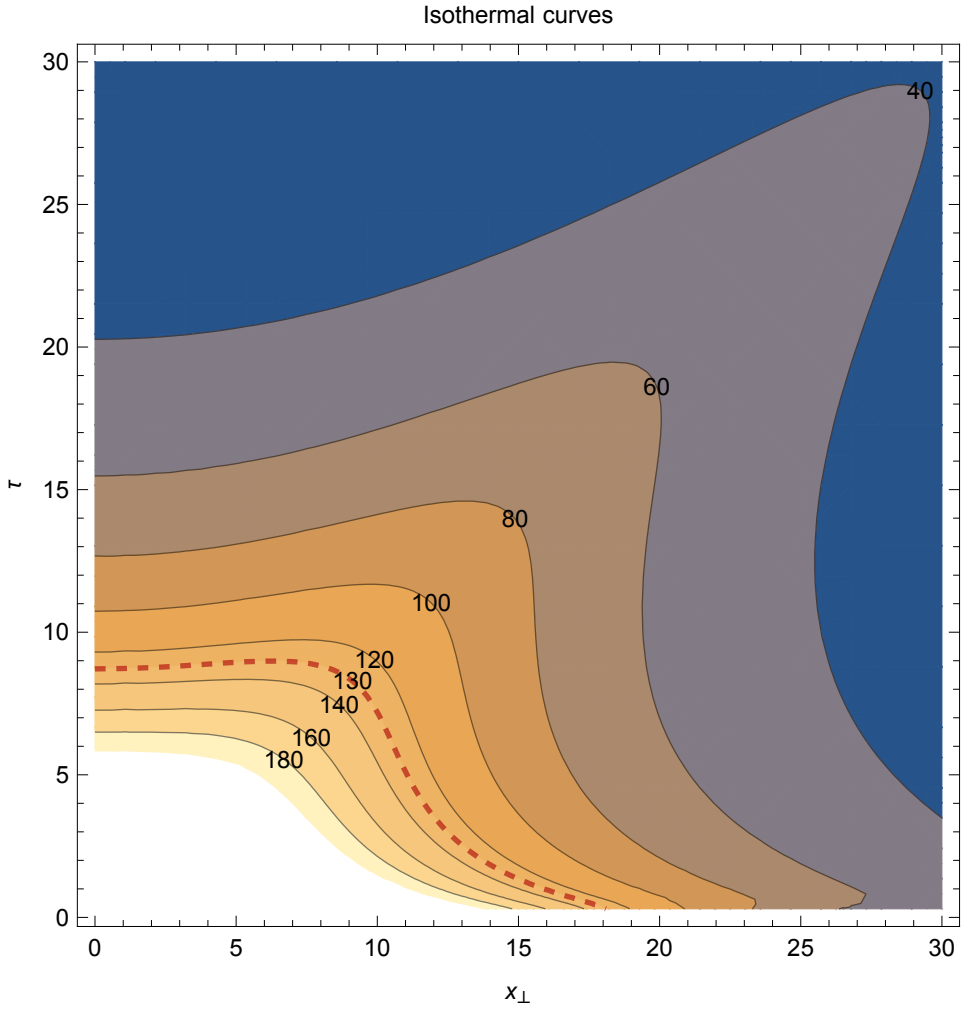

Figure 9: Here we show some isothermal curves for Gubser's solution, where now $q^{-1} = 6.4$ fm and $\hat{T}_0 = 10.8$ as obtained in the Freeze-out section for getting the best spectra. We plot here the proper time τ against the coordinate $x_\perp$ in the transverse plane. The highlighted contour $T_f = 130$ MeV, is the one we pick for our freezeout surface $\rightarrow \tau_f(x_\perp)$.

We can plot Gubser's temperature profile (the isothermal curves, that is) when we pick values for q and $\hat{T}_0$ (see next section), the result is shown in Fig 9.

One might realize that Gubser's solution is rotationally invariant around the $\hat{z}$-axis and therefore cannot be directly applicable to collisions with a non-zero impact parameter b (which we set to 7 fm). We stress therefore again that our intention is merely to obtain a order of magnitude for the anisotropic flows, and not a precise calculation.

4.3 FREEZOUT AND SPECTRA

4.3.1 *Introduction*

In this section the freezeout procedure will be described, which is used to create spectra for pions and protons from Gubser's flow. We shall compare this to experimentally obtained spectra from LHC.
What remains is to fix the constants q and $\hat{T}_0$, these together determine the initial conditions of the QGP. They determine the initial temperature profile at the time when our hydrodynamics become viable in describing the expansion of the plasma.
If we look at appropriate hydrodynamic calculations, see [19], it becomes clear that at a time of $\tau = 0.6$ fm we expect the temperature to be around 445-485 MeV. Note however that we can't use this temperature to fix our constants, since the used Woods-Saxon distribution is quite different from our temperature profile (Gubser's solution).

So our approach will be somewhat different and we start by noting that q and $\hat{T}_0$ together determine, implicitly, the velocity profile at the end of the hydrodynamic expansion. This then determines the hadron spectra after the freezeout. So to find out appropriate values for our constants we will create proton and pion spectra from our solution and compare it with experimentally found spectra. These are taken from 20-30% centrality, since we used this same centrality with our model as well.

4.3.2 *Formalism*

The goal we want to achieve is to go from the degrees of freedom of hydrodynamics to measurable quantities. This is called the freezeout. We shall simply work towards our desired result, for a detailed review of relativistic viscous hydrodynamics see Ref. [21]. The hydrodynamics that are developed deal with quantities like energy density and fluid velocity. The experiment, however, deals with measured quantities like the momentum distribution of protons and pions.
We expect the freezeout to happen when the temperature becomes so

low that the interactions can no longer hold thermal equilibrium. For our QGP, this happens as it cools and the viscosity becomes stronger, until the viscous corrections cause the hydrodynamic description to be no longer viable, see also [21].

Now, we can't simply calculate this complicated transition with viscous corrections and instead a widely used technique is to implement an isochronous and isothermal freezeout. This is done by defining a three-dimensional hypersurface Σ with a normal vector $d\Sigma^\mu$. The total amount of particles after the freezeout is then given by the particle current through the surface Σ^μ.
While this method seems fairly unrealistic, quite proper results can be obtained from it (at least for the correct order of magnitude) [21].

The link between the hydrodynamic variables and the desired spectra is then given by the Cooper-Frye freezout procedure [20]. In summary we can write it as Equation 62.

$$S_i = \left(p^0 \frac{d\,N_i}{d^3\,p} \right) = \frac{d_i}{(2\pi)^3} \int d\Sigma_\mu \; p^\mu \; f(\vec{p}, t, \vec{x}) \tag{62}$$

Here S_i is the spectrum of species i, p^0 is the zeroth (time) component of the four-momentum, f states a distribution function and d_i is defined as:

$$d_i = (2s_i + 1)(2g_i + 1) \tag{63}$$

With s_i the spin of the particle and g_i the isospin. In practice, the term d_i denotes the degeneracy of the particle being looked at.
The area element of the freezeout surface, $d\Sigma_\mu$, for a surface parameterized in x,y,z would look as in Equation 64.

$$d\Sigma_\mu = \epsilon_{\mu\alpha\beta\gamma} \frac{\partial\Sigma^\alpha}{\partial x} \frac{\partial\Sigma^\beta}{\partial y} \frac{\partial\Sigma^\gamma}{\partial z} dx\, dy\, dz \tag{64}$$

With $\epsilon_{\mu\alpha\beta\gamma}$ the Levi-Civita symbol, defined as +1 for even permutations, -1 for uneven permutations and 0 otherwise. At this point we are ready to apply this formalism of the freezeout to our specific situation.

Note that this is not a tensor but a tensor density. To make it a tensor it should be multiplied with the square root of the metric's determinant.

4.3.3 *Applied freezeout*

For our purposes we shall be looking at protons and pions, since these are proper particles to measure in experiment. In order to get a full expression for Equation 62 we need to define first our four momentum. We give these in terms of the mass of the particle (m_i), the transverse

momentum (p_T), rapidity (Y) and the azimuthal angle in momentum space (ϕ_p), see Equation 65. If not immediately apparent, these can be quickly derived using simple sketches and remember from the introductory chapter that $\cosh(Y) = \gamma$, where γ is the Lorentz factor $1/\sqrt{1-v^2}$.

$$\begin{aligned} p^0 &= m_T \cosh Y \\ p^z &= m_T \sinh Y \\ p^y &= p_T \sin\phi_p \\ p^x &= p_T \cos\phi_p \end{aligned} \tag{65}$$

Where $m_T = \sqrt{p_T^2 + m_i^2}$. We also note that we can now expand the spectra S_i as (see also Equation 1):

$$\begin{aligned} S_i = \left(p^0 \frac{d^3 N_i}{d^3 p}\right) = \frac{d^3 N_i}{p_T \, dY \, dp_T \, d\phi_p} = \\ = v_0(1 + 2v_1 \cos(\phi_p - \pi) + 2v_2 \cos(2\phi_p) + ...) \end{aligned} \tag{66}$$

The parameters v_1, v_2 etc. are the directed, elliptic flow and higher orders. These depend on Y and p_T. Note the factor π in the v_1 term. This is due to the fact that usually the directed flow is defined to be positive for $Y > 0$ when the flow is deflecting away from the collision origin. If we compare this with Fig 4 we see that our definition is just the other way around, resulting in the factor π in Equation 66.

As for our solution, we know it is azimuthally symmetric and boost invariant, which means it is independent of Y and ϕ_p. This means the only non-vanishing parameter will be v_0 and it is given as (see Equation 66):

$$v_0 = \frac{1}{2\pi p_T} \frac{d^2 N}{dY \, dp_T}$$

So, as stated earlier, we now want to calculate the spectra (v_0 in this case) for pions and protons. To do this we need to take an isothermal surface T_f at which the freezeout happens. With this we can retrieve $\tau_f(x_\perp)$ from $T(x_\perp, \tau_f) = T_f$, with $T(x_\perp, \tau_f)$ Gubser's solution given in Equation 61. Just as in [1] we will pick $T_f = 130$ MeV, as it turns out this will give reasonable results.
It now remains only to pick a distribution f, as seen in Equation 62. In the view of wanting a analytic solution we take a Boltzmann distribution as $f = Exp(\frac{p^\mu u_\mu}{T_f})$. So taking this all into account we get for the Cooper-Frye procedure our result in Equation 67.

$$S_i = \left(p^0 \frac{d^3 N_i}{d^3 p}\right) = -\frac{d_i}{(2\pi)^3} \int d\Sigma_\mu \, p^\mu e^{\frac{p^\mu u_\mu}{T_f}} \tag{67}$$

The minus sign is due to the fact that we want to have positive result (see below). Further we note that u_μ is the found four-velocity of Gubser's solution, and d_i denotes the degeneracy of the involved particle.
So we have now a freezout surface $\Sigma^\mu = (\tau_f(x_\perp), \eta, x_\perp, \phi)$ (don't confuse ϕ with ϕ_p as seen in Equation 65) with τ_f the solution of earlier said $T(x_\perp, \tau_f) = T_f$, see Fig 9 at $T_f = 130$ MeV. The next step is to determine the area element $d\Sigma_\mu$ of the freezeout surface. In our coordinate system we have the following definition of the area element (see also Equation 64):

$$d\Sigma_\mu = -\epsilon_{\mu\nu\lambda\rho} \frac{\partial\Sigma^\nu}{\partial\eta} \frac{\partial\Sigma^\lambda}{\partial x_\perp} \frac{\partial\Sigma^\rho}{\partial\phi} \sqrt{-g}\, d\eta\, dx_\perp\, d\phi \tag{68}$$

Note that there is no dt in $d\Sigma_\mu$, it is an isochronous surface.

Where $\sqrt{-g}$ is the determinant of the metric. In our case we have the following metric, which can also be seen from Equation 46:

$$ds^2 = -d\tau^2 + \tau^2\, d\eta^2 + x_\perp^2\, d\phi^2 + dx_\perp^2 \tag{69}$$

It follows now that the determinant will be given as $\sqrt{-g} = x_\perp\, \tau_f$. Note that the f in τ_f is merely to indicate that it belongs to the freezeout surface.
Another trick we use is that since $dT = 0$ we have that:

$$\begin{aligned} dT &= \frac{\partial T}{\partial x_\perp} dx_\perp + \frac{\partial T}{\partial \tau} d\tau = 0 \\ R_f &\equiv -\frac{\partial \tau_f}{\partial x_\perp} = \left.\frac{\partial T/\partial x_\perp}{\partial T/\partial \tau}\right|_{T_f} \end{aligned} \tag{70}$$

Using above expression, the metric and completing the implicit summation in Equation 68 we get our expression for the area element as given in Equation 71.

$$d\Sigma_\mu = (-1, 0, R_f, 0)\, x_\perp\, \tau_f\, d\eta\, dx_\perp\, d\phi \tag{71}$$

What remains to be done now is work out the summations $p^\mu u_\mu$ and $d\Sigma_\mu p^\mu$. This is easily done by noting that the four-velocity u^μ has only two components, u^τ and $u^\perp$ (see Equation 56 and Equation 57). The summations can then be written as:

$$\begin{aligned} p^\mu\, u_\mu &= g_{\mu\nu}\, p^\mu\, u^\nu \\ d\Sigma_\mu\, p^\mu &= g_{\mu\nu}\, d\Sigma^\nu\, p^\mu \end{aligned}$$

We also know from Equation 71 that $d\Sigma_\mu$ will only have a τ and a $\perp$ component, so we need only to raise some indices with the metric

as in Equation 69. To get, however, the four momentum p^μ in terms of a τ and $\perp$ component we use the standard coordinate transformation. Note that our Minkowsky metric (written as $\eta_{\mu\nu}$) is picked as $(-1, 1, 1, 1)$.

$$p_{x'} = \frac{\partial x^\alpha}{\partial x'} p_\alpha = \eta_{\alpha\beta} \frac{\partial x^\alpha}{\partial x'} p^\beta$$

Here p^β represents the found components of our four-momentum as in Equation 65. Using the above expression we can write out the summations.

$$p^\mu u_\mu = -m_T \cosh(Y - \eta)\, u^\tau + p_T \cos(\phi_p - \phi)\, u^\perp \tag{72}$$

$$\begin{aligned} d\Sigma_\mu p^\mu = &-m_T \cosh(Y - \eta)\, x_\perp\, \tau_f(x_\perp)\, d\eta\, dx_\perp\, d\phi \\ &-p_T R_f \cos(\phi_p - \phi)\, x_\perp\, \tau_f(x_\perp)\, d\eta\, dx_\perp\, d\phi \end{aligned} \tag{73}$$

With this now complete, we can input both summations into Equation 67 and finally write our final integral expression for the spectra S_i.

$$\begin{aligned} S_i = \frac{d_i}{(2\pi)^3} \int_0^{x_f} dx_\perp\, \tau_f(x_\perp) \int_{-\infty}^{\infty} d\eta\, e^{-\frac{m_T u^\tau}{T_f} \cosh(Y-\eta)} \\ \int_0^{2\pi} d\phi\, e^{\frac{p_T u^\perp}{T_f} \cos(\phi_p - \phi)} \left(m_T \cosh(Y - \eta) + R_f\, p_T \cos(\phi_p - \phi)\right) \end{aligned} \tag{74}$$

Here x_f denotes the final $x_\perp$ coordinate after which $\tau_f(x_\perp)$ will be (very close to) zero, see also Fig 9.

4.3.4 *Calculating the spectra*

Now that we have the integral expression we wish to solve it. To do this we first note the following definitions of some Bessel functions.

$$I_\nu(z) = \frac{1}{\pi} \int_0^\pi e^{z \cos(t)} \cos(\nu t)\, dt \tag{75}$$

$$K_\nu(z) = \int_0^\infty e^{-z \cosh(t)} \cosh(\nu t)\, dt \tag{76}$$

If compared to Equation 74 we can see that the η and ϕ integrals can thus be solved analytically. To do this we just do some simple coordinate transformations and adjusting of the boundaries (note that Y and ϕ_p are constants in the integrals), which gives our final expression, as given in Equation 77.

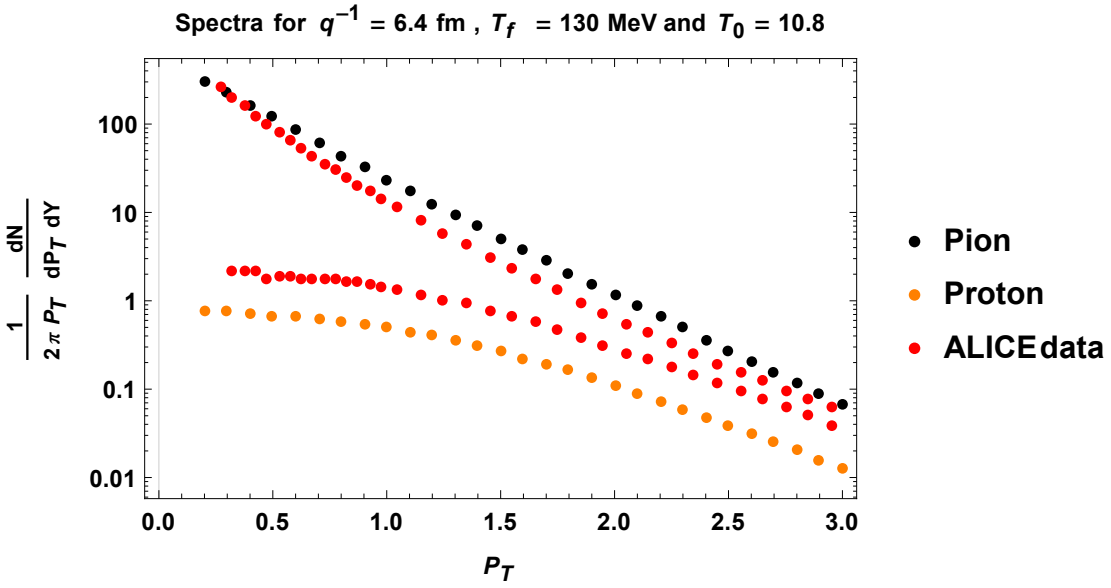

Figure 10: These are the spectra of protons and pions from Gubser's solution and the experimentally obtained spectra by the ALICE collaboration [22]. Since we incorperated no chemical potential for baryon number or isospin, the spectra for protons and antiprotons are the same, just as negatively and positively charged pions.

$$
\begin{aligned}
S_i = p^0 \frac{d^3 N_i}{d^3 p}\bigg|_{Gubser} &= \frac{d_i}{2\pi^2}\int dx_\perp \tau_f(x_\perp) \\
&\times \left[m_T K_1\left(\frac{m_T u^\tau}{T_f}\right) I_0\left(\frac{p_T u^\perp}{T_f}\right)\right. \\
&\left. + R_f p_T K_0\left(\frac{m_T u^\tau}{T_f}\right) I_1\left(\frac{p_T u^\perp}{T_f}\right)\right]
\end{aligned}
\tag{77}
$$

The degeneracy $d_i = 2$ for both the pions and the protons, since the above expression does not differentiate between the two. The only thing that remains is to pick the constants q and $\hat{T}_0$ and after this numerically integrate the $x_\perp$ integral. We select our values for the constants by comparing it to experimentally obtained spectra for LHC heavy ion collisions at 20-30% percent centrality, as measured by the ALICE collaboration, see Ref. [22].
After doing this, the best results obtained were at $q = \frac{1}{6.4}$ fm^{-1} and $\hat{T}_0 = 10.8$, which is the same result as obtained in [1]. The comparison is shown in Fig 10.

4.4 CONCLUDING

In this chapter we have derived a hydrodynamic model for the expansion of the QGP. And although there were many simplifying assumptions in Gubser's model and the use of an isochronous, isothermal

freezeout surface, a reasonable spectrum was obtained in Fig 10.
It is possible to get a little better description of the pion spectrum by using a T_f of 120 or 110 MeV, but this will go at the cost of a worse description of the proton spectrum.

What remains to be done now is to incorporate the electromagnetic field obtained in the previous chapter. We combine both and can then see what the influence of the electromagnetic field is on the expansion of the Quark Gluon Plasma.

5 DIRECTED FLOW

5.1 INTRODUCTION

As mentioned in the first introductory chapter, Section 1.4.1, we shall at this point incorporate the electromagnetic fields and figure out the effect on the expansion of the QGP. In this chapter we will deal with the directed flow.

To summarize, we want to obtain the fluid velocity V^μ, which contains both the expansion due to Gubser's model (Chapter 4) and the electromagnetic field (Chapter 3). We do this by doing a Lorentz boost to the local fluid restframe in which applies $u'^\mu = 0$. At this point we shall solve the equation of motion given in Equation 80, to get the velocity due to the electromagnetic fields $\vec{v}'$.
We do this for up quarks ($q = \frac{2}{3}e$) and anti down quarks ($q = \frac{1}{3}e$), which will apply to the positively charged particles later on. We simply add these two together and divide by two to get our velocity. For negatively charged particles we use then the anti up and down quarks. Note that we assume that there are equal distributions of up and down quarks and thus ignore any chemical potential induced by the differences. The negative particles will just be characterized by $-\vec{v}'$.

5.2 LORENTZ TRANSFORM

The Lorentz boost is then $\Lambda(-\vec{u})$. The general matrix form of a boost of $\vec{\beta}$ is shown in Equation 78.

$$\begin{bmatrix} \gamma & -\gamma\beta_x & -\gamma\beta_y & -\gamma\beta_z \\ -\gamma\beta_x & 1+(\gamma-1)\frac{\beta_x^2}{\beta^2} & (\gamma-1)\frac{\beta_x\beta_y}{\beta^2} & (\gamma-1)\frac{\beta_x\beta_z}{\beta^2} \\ -\gamma\beta_y & (\gamma-1)\frac{\beta_y\beta_x}{\beta^2} & 1+(\gamma-1)\frac{\beta_y^2}{\beta^2} & (\gamma-1)\frac{\beta_y\beta_z}{\beta^2} \\ -\gamma\beta_z & (\gamma-1)\frac{\beta_z\beta_x}{\beta^2} & (\gamma-1)\frac{\beta_z\beta_y}{\beta^2} & 1+(\gamma-1)\frac{\beta_z^2}{\beta^2} \end{bmatrix} \tag{78}$$

We also note that in our center of mass frame we have the electromagnetic field tensor as in Equation 79. With components E_x and B_y as given in Equation 51 and Equation 52, where now of course $\tau = \tau_f(x_\perp)$.

$$F^{\mu\nu} = \begin{pmatrix} 0 & -E_x & 0 & 0 \\ E_x & 0 & 0 & B_y \\ 0 & 0 & 0 & 0 \\ 0 & -B_y & 0 & 0 \end{pmatrix} \tag{79}$$

5.3 COMPUTING V^μ

Now utilize the found velocities Equation 56 and Equation 57 along with the metric Equation 69 to do some algebra and then find that in the local fluid rest frame all components of $\vec{E}'$ and $\vec{B}'$ are non-vanishing.
With these fields determined, it is time to solve the equation of motion, Equation 80. Where we pick the charge q as described in the introduction.

$$m \frac{d\vec{v}'}{dt} = q\vec{E}' + q\vec{v}' \times \vec{B}' - \mu\, m\, \vec{v}' = 0 \tag{80}$$

This gives us the local velocity due to electromagnetic effects $\vec{v}'$. We can now use a Lorentz transformation back, $\Lambda(\vec{u})$, to get to the center of mass frame again, resulting in our expression for the total four-velocity V^μ.
At this point it is also possible to check the assumption that $|\vec{v}| << |\vec{u}|$, to do this we can see what the difference between V^μ and u^μ is. As it turns out this is maximally 0.001 in the range of $(x_\perp, \eta, \phi)$ space. So the assumption was a valid one.

5.4 DIRECTED FLOW CALCULATION

Having obtained our four-velocity we can now follow the freezout procedure as described in the chapter of Hydrodynamics, but instead of u^μ we use V^μ. Note that this new four velocity *does* have a ϕ and η component.
First we look at the expanded spectra as in Equation 66. From this definition we get our expression for v_1.

This expression is easily checked by writing out S_i and computing the integral.

$$v_1(p_T, Y) = \frac{\int_{-\pi}^{\pi} d\phi_p \, \cos(\phi_p - \pi)\, S_i(p_T, Y, \phi_p)}{2\pi v_0} \tag{81}$$

Due to the small difference between V^μ and u^μ it is very reasonable to take the v_0 in above expression as the found v_0 in previous chapter, Equation 77. And S_i is in this case given by Equation 67, but with the four velocity u_μ replaced by the newly found one of course. The expression that results is shown in Equation 82.

$$S_i = \frac{d_i}{(2\pi)^3}\int d\eta\, dx_\perp\, d\phi\, x_\perp\, \tau_f(x_\perp)\, e^{-\frac{m_T}{T_f}(V^\tau \cosh(Y-\eta)-V^\eta\, \tau_f\, \sinh(Y-\eta))} \times \Big[m_T\, \cosh(Y-\eta)\, e^{\frac{p_T}{T_f}(V^\perp \cos(\phi_p-\phi)+V^\phi\, x_\perp\, \sin(\phi_p-\phi))} + p_T\, R_f \cos(\phi_p-\phi)\, e^{\frac{p_T}{T_f}(V^\perp \cos(\phi_p-\phi)+V^\phi\, x_\perp\, \sin(\phi_p-\phi))}\Big] \quad (82)$$

This equation for S_i can now be plugged back into Equation 81. There are at this point four integrals to be done and it turns out we can complete the ϕ_p integral analytically with Bessel and hypergeometric functions, with help from Ref. [10]. The tedious result that we have to work with is shown below.

$$v_1(p_T, Y) = \frac{1}{2\pi v_0}\frac{d_i}{(2\pi)^2}\int d\eta\, dx_\perp\, d\phi\, x_\perp\, \tau_f(x_\perp)\, e^{-\frac{m_T}{T_f}(V^\tau \cosh(Y-\eta)-V^\eta\, \tau_f\, \sinh(Y-\eta))} \times \Big[\Big(V^\perp \cos(\phi) - x_\perp\, V^\phi\, \sin(\phi)\Big) \times \Big\{\frac{m_T\, \cosh(Y-\eta)}{\sqrt{W}}\, I_1\Big(\frac{p_T}{T_f}\sqrt{W}\Big) + R_f\, p_T\, \frac{V^\perp}{W}\Big(I_o\Big(\frac{p_T}{T_f}\sqrt{W}\Big) - \Psi_2\Big(\frac{p_T^2}{4T_f^2}\, W\Big)\Big)\Big\} + \frac{1}{2}\, R_f\, p_T \cos(\phi)\, \Psi_2\Big(\frac{p_T^2}{4T_f^2}\, W\Big)\Big] \quad (83)$$

Here $W \equiv \left(V^\perp\right)^2 + x_\perp^2\, \left(V^\phi\right)^2$. All other integrals shown in Equation 83 have to be done numerically.

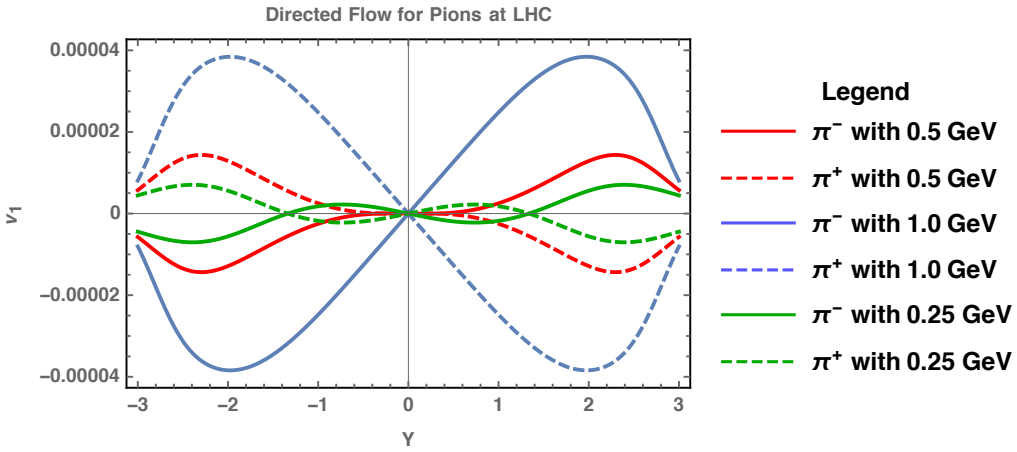

Figure 11: The directed flow at fixed transverse momentum for pions at LHC. Note the difference for π^- and π^+ due to the charge dependency of v_1. This and all other produced results are for a 20-30% centrality.

5.5 FIXED AND INTEGRATED p_T

First thing we do is numerically integrate the found Equation 83 for a fixed p_T and thereby gain a result for v_1 against the rapidity. The results are shown in Fig 11 and Fig 12, for pions and (anti)protons respectively. Note that for protons the directed flow actually changes sign when the transverse momentum is increased enough. The reason for this is still a point of debate, but the most likely cause is the interplay of the Hall and Faraday effect (see also next section).
Just for completeness we repeat the used constants in these numerical integrations.

$\pm Y_0 = \pm 8$	Beam rapidity
$\sigma = 0.023\ \text{fm}^{-1}$	Conductivity
$\hat{T}_0 = 10.8$ and $q^{-1} = 6.4$ fm	Initial temperature profile
$\mu m = \frac{1}{2}\pi\sqrt{\lambda}\left(\frac{3}{2}T_c\right)^2$	Drag coefficient
$\lambda = 6\pi$	t' Hooft coupling
$T_c = 170$ MeV	Crossover temperature
$T_f = 130$ MeV	Freezeout temperature

Note that in all these results that we show, that it is merely the charge dependent part of the directed flow. There is most likely another bigger contribution caused by initial asymmetries in the collision.

It is even possible (not easily) to numerically integrate the found expression, Equation 83, over p_T distributions. The results we obtained are shown in Fig 13, Fig 14 and Fig 16.
Also we produced results for very high p_T ranges as ALICE (at LHC) allows us to discriminate up to 5 GeV see Fig 15. For a short discussion how we numerically integrated expressions like this, also over p_T distributions, see Appendix A.

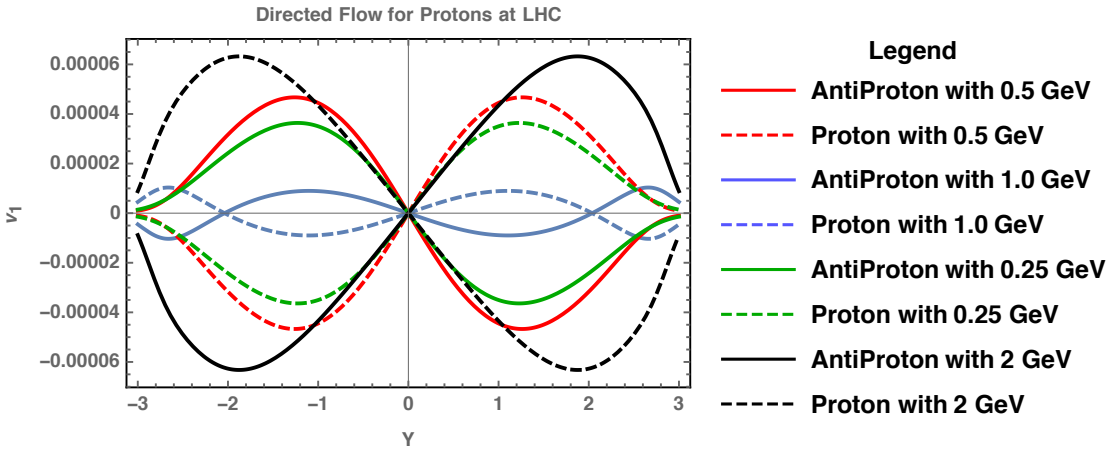

Figure 12: The directed flow at fixed transverse momentum for protons at LHC. The charge dependency is again seen, but now for the proton and antiproton. It can be seen that the directed flow for increasing p_T does behave differently than for pions.

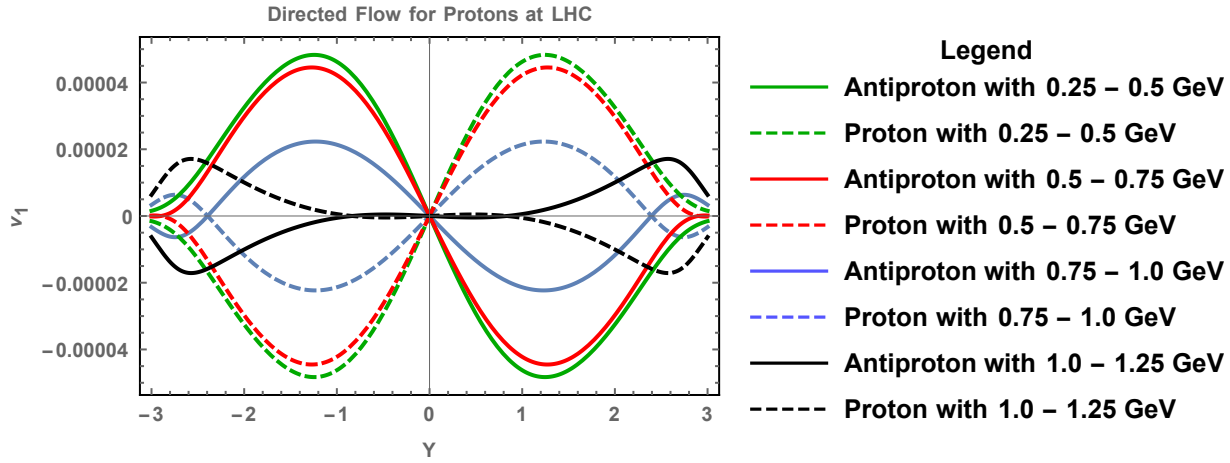

Figure 13: Here we show the directed flow for (anti)protons for smaller p_T ranges at LHC.

5.6 HALL AND FARADAY

Another interesting concept to look at is the different contributions to the total v_1 by the different magnetic effects.
As stated in previous chapters we have a Faraday and a Hall effect. We can eliminate the Hall effect from our calculations to obtain the directed flow due to only the Faraday effect. We show our results in Fig 17.
As can be seen, the Hall and Faraday effect are different in sign and work against each other.

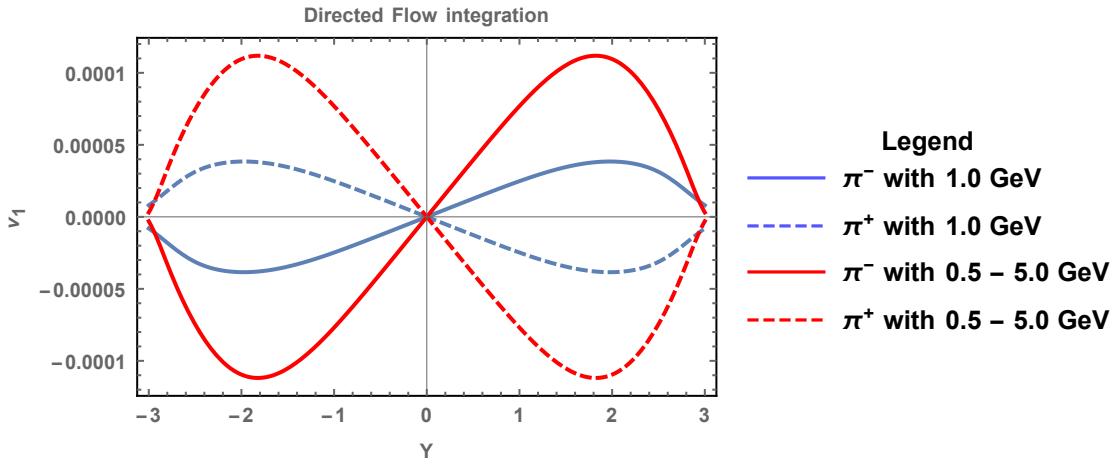

Figure 14: Here we show the directed flow integrated from p_T from 0.5 - 5.0 GeV compared to the directed flow at fixed p_T = 1.0 GeV. This integration is especially important for practical aspects, as we also integrate over this p_T range in experimental detection.

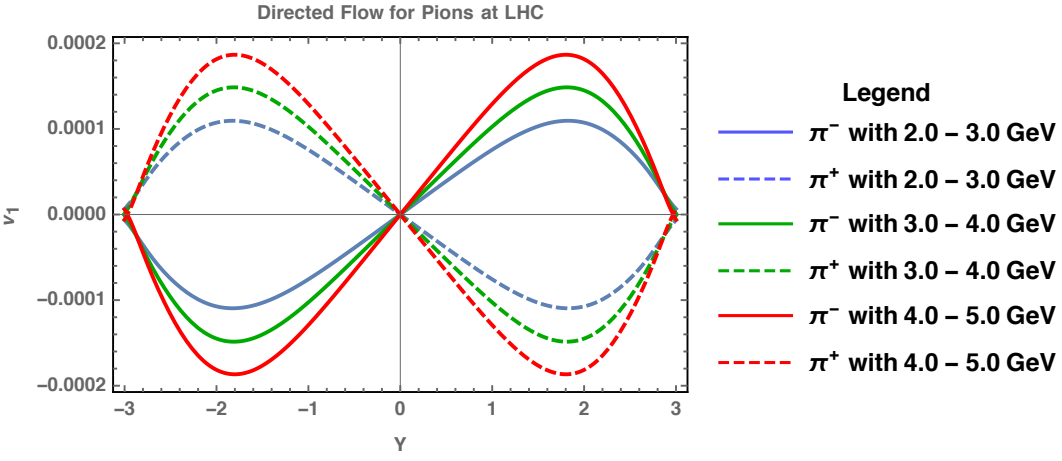

Figure 15: This plot shows the directed flow for pions at LHC for especially high p_T ranges. This is because at ALICE we can discriminate up to 5 GeV in transverse momentum.

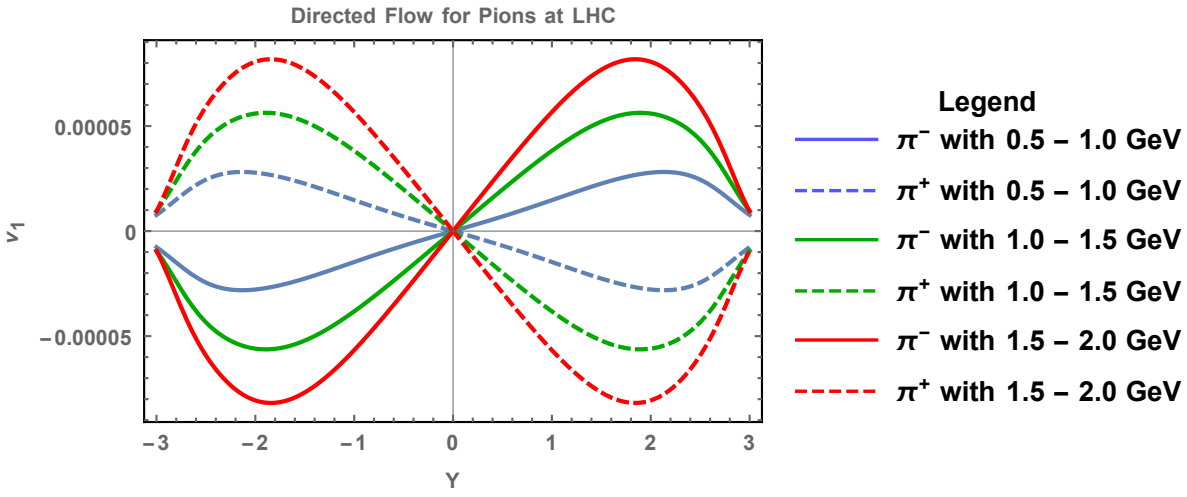

Figure 16: The directed flow at some larger transverse momentum bins for pions at LHC.

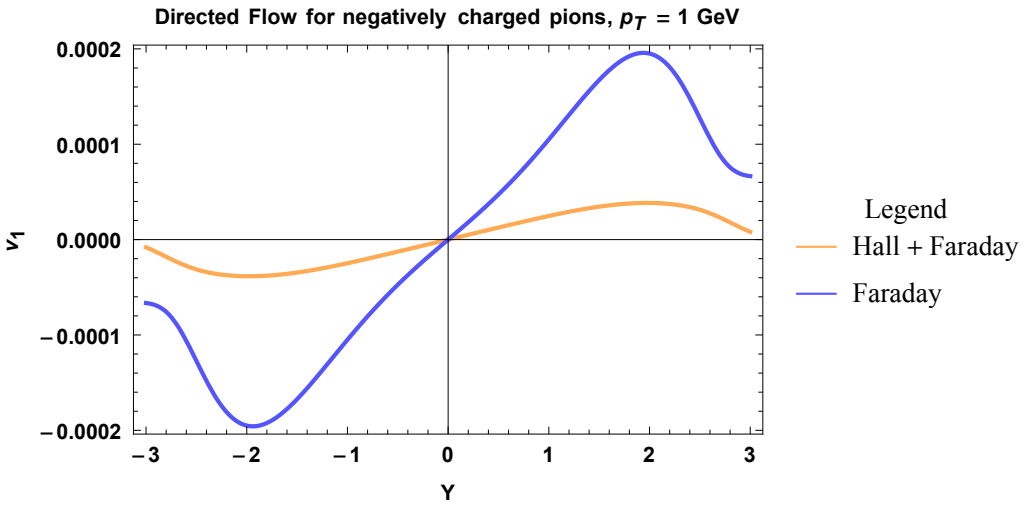

Figure 17: Here we show the directed flow due to only the Faraday effect and both the Faraday and Hall effect. It is apparent that the Hall and Faraday effect are of opposite sign.

6 ELLIPTIC FLOW AND EXPRESSIONS FOR v_n

6.1 INTRODUCTION

The results for the directed flow were obtained in previous section. Our next goal is to figure out an order of magnitude estimate for the elliptic flow due to the electromagnetic fields.
To do this we first need a formula like Equation 83 to calculate v_2. It turns out we can do even better, in this chapter we will start by deriving an expression for obtaining any flow-component v_n. With this we will study the elliptic flow.

6.2 GENERALIZATION FOR ANY FLOW-COMPONENT

We can generalize the calculation we did for v_1 to higher harmonics v_n, as is shown in Equation 84.

$$v_n(p_T, Y) = \frac{\int_{-\pi}^{\pi} d\phi_p \cos(n\phi_p) S_i(p_T, Y, \phi_p)}{\int_{-\pi}^{\pi} d\phi_p S_i(p_T, Y, \phi_p)} = \frac{\int_{-\pi}^{\pi} d\phi_p \cos(n\phi_p) S_i(p_T, Y, \phi_p)}{2\pi v_0} \tag{84}$$

This expression can again be checked by filling in the definition of the spectrum S_i, see Equation 66. The expression in the numerator of Equation 84 can be rewritten using the found results in previous chapter (only now for v_n), Equation 81 and Equation 83.

$$\begin{aligned} &\int_{-\pi}^{\pi} d\phi_p \cos(n\phi_p) S_i(p_T, Y, \phi_p) = \\ &\frac{g_i}{(2\pi)^3} \int d\eta\, dx_\perp\, d\phi_{x_\perp} \tau_f e^{-\frac{m_T}{T_f}(V^\tau \cosh(Y-\eta) - V^\eta \tau_f \sinh(Y-\eta))} \\ &\times (m_T \cosh(Y-\eta) M_n + R_f p_T N_n) \end{aligned} \tag{85}$$

Just to remind, R_f is given by the ratio $R_f = -\partial\tau_f(x_\perp)/\partial x_\perp$. Further, M_n and N_n read:

$$M_n = \int_{-\pi}^{\pi} d\phi_p \cos(n(\phi_p + \phi)) e^{\frac{p_T}{T_f}(V^\perp \cos\phi_p + V^\phi x_\perp \sin\phi_p)} \tag{86}$$

$$N_n = \int_{-\pi}^{\pi} d\phi_p \cos(n(\phi_p + \phi)) \cos\phi_p e^{\frac{p_T}{T_f}(V^\perp \cos\phi_p + V^\phi x_\perp \sin\phi_p)} \tag{87}$$

For convenience later on we define the following parameters:

$$A \equiv \frac{p_T V^{\perp}}{T_f}, \qquad B \equiv \frac{p_T V^{\phi} x_{\perp}}{T_f} \tag{88}$$

6.2.1 *Expressions for* N_n *and* M_n

We can at this point use several equations on p. 709, Ref. [10]. This leads to the following result.

$$\int_{-\pi}^{\pi} d\phi_p e^{A\cos\phi_p + B\sin\phi_p} = 2\pi I_0\left(\sqrt{A^2+B^2}\right) \tag{89}$$

Where I_0 is the Bessel I-function. For the case of v_2 we need M_2 and N_2.

$$\begin{aligned} M_2 &= 2\pi\left[\cos(2\phi)\left(\frac{d^2}{dA^2} - \frac{d^2}{dB^2} - 2\sin(2\phi)\frac{d}{dA}\frac{d}{dB}\right)\right] I_0\left(\sqrt{A^2+B^2}\right) \\ N_2 &= \frac{d}{dA} M_2 \end{aligned}$$

It is however not as nice of an expression. As it turns out we can also rewrite M_n and N_n in a simpler form using again formulae on p. 709 of Gradsteyn-Rhyzik. First we use the following relations:

$$\begin{aligned} \cos(n(\phi_p+\phi)) &= \cos(n\phi_p)\cos(n\phi) - \sin(n\phi_p)\sin(n\phi) \\ \cos(n(\phi_p+\phi))\cos(\phi_p) &= \frac{1}{2}\cos(n\phi)\left(\cos(\phi_p(n+1)) + \cos(\phi_p(n-1))\right) \\ &\quad -\frac{1}{2}\sin(n\phi)\left(\sin(\phi_p(n+1)) + \sin(\phi_p(n-1))\right) \end{aligned}$$

We can now fill these expressions into Equation 86 with Gradsteyn-Rhyzik and get for the cos term:

$$\begin{aligned} &\int_0^{2\pi} e^{A\cos(\phi_p)+B\sin(\phi_p)}\cos(n\phi_p)\,d\phi_p = \\ &\frac{\pi}{(A^2+B^2)^{\frac{n}{2}}}\left(I_n\left(\sqrt{A^2+B^2}\right)\left((A+iB)^n + (A-iB)^n\right)\right) \end{aligned} \tag{90}$$

Now, the solution of Equation 90 can be rewritten as,

$$2\pi\cos\left(n\arctan\left(\frac{B}{A}\right)\right) I_n\left(\sqrt{A^2+B^2}\right) = 2\pi\cos(n\,\xi)\,I_n(\zeta) \tag{91}$$

Note that we defined $\xi = \arctan\left(\frac{B}{A}\right)$ and $\zeta = \sqrt{A^2+B^2}$. Doing this same calculation for the sin term and adding them together (with the factors $\cos(n\phi)$ and $\sin(n\phi)$) yields our result,

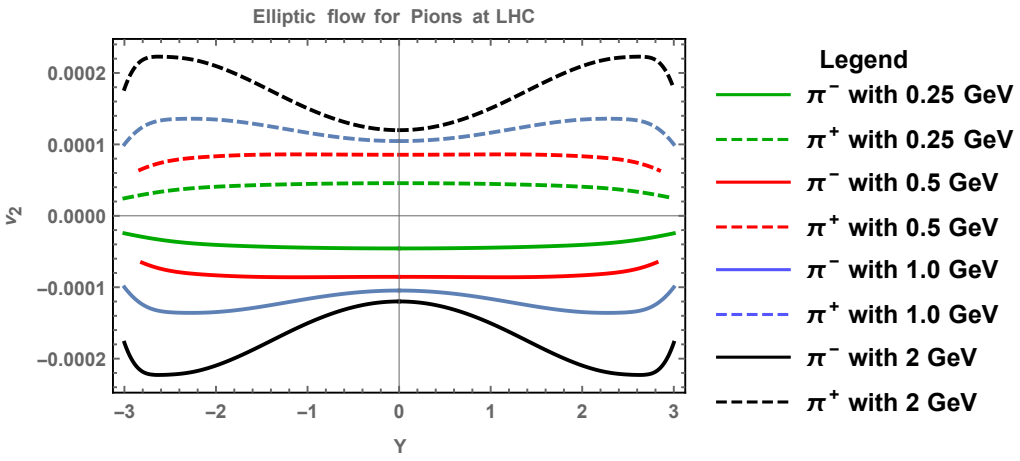

Figure 18: The elliptic flow at fixed transverse momentum for protons at LHC plotted against rapidity Y. Note again that all the results derived are for a 20-30% centrality.

$$M_n = 2\pi \cos(n(\phi + \xi))\, I_n(\zeta) \tag{92}$$

The same procedure can be repeated, with Equation 90, to obtain a result for the N_n integral.

$$N_n = \pi\,(\cos[(n-1)\xi + n\phi)]\, I_{n-1}(\zeta) + \cos[(n+1)\xi + n\phi)]\, I_{n+1}(\zeta)) \tag{93}$$

The results for M_n and N_n can now be plugged back into Equation 85 and Equation 84. We then have a complete expression for any flow component v_n.

6.3 ELLIPTIC FLOW

It is now possible to get an expression for the elliptic flow as we use the expression for v_n from previous section with $n = 2$, see Equation 85 (with the factor $\frac{1}{2\pi v_0}$).
Once again we shall numerically integrate this expression, first for fixed transverse momentum as shown in Fig 18 and Fig 19.

We also managed to obtain results for several transverse momentum bins. These are shown in Fig 20 and Fig 21.

Most noteworthy is that it seems that the elliptic flow caused by the electromagnetic effects is about an order of magnitude bigger than the directed flow. Also, the elliptic flow doesn't change sign for $\pm Y$ because of the definition of it, for intuitive understanding it might help to look at Fig 2.

For a very detailed review on elliptic flow (and measuring it) see Ref. [23].

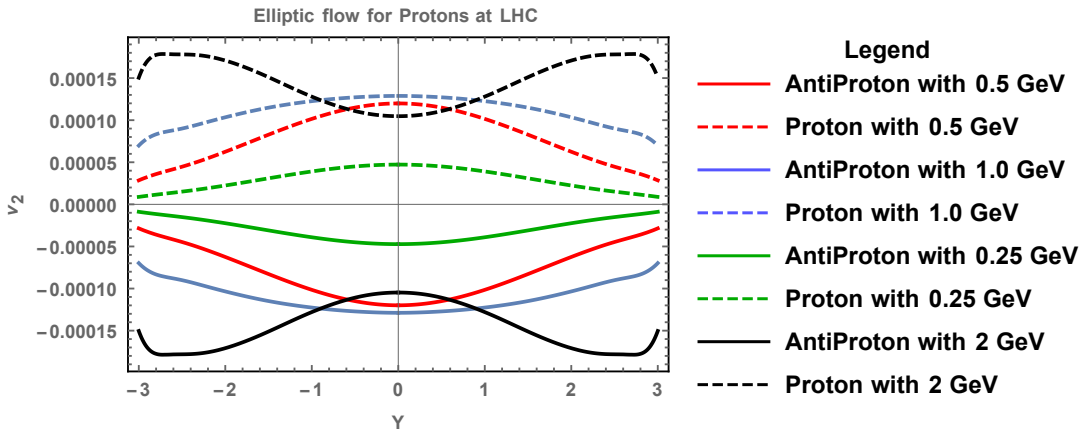

Figure 19: The elliptic flow at fixed transverse momentum for protons at LHC. The charge dependency is again seen, but now for the difference proton and antiproton.

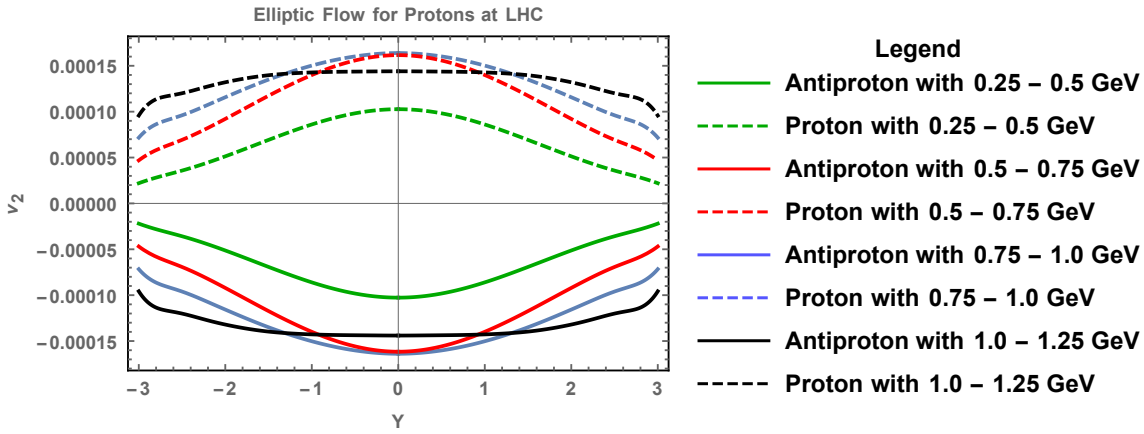

Figure 20: Here we show the elliptic flow for (anti)protons for some small p_T ranges at LHC, plotted against the momentum space rapidity Y.

Note that again we present the charge dependent part of the elliptic flow that is caused by the effects of the electromagnetic field on the expansion of the QGP. The, presumably larger, elliptic flow caused by initial asymmetries is in reality added to this. The contribution of these initial asymmetries will however not be charge dependent and as such it would still be possible to detect our charge dependent elliptic flow.
For example, looking at Fig 18, if the charge independent contribution at $Y > 0$ is bigger than zero we shall obtain in measurement that $v_2(\pi^+) > v_2(\pi^-)$ for any of these transverse momenta.

Another result obtained is the elliptic flow plotted against the transverse momentum at mid rapidity ($Y = 0$). We show this in Fig 22.

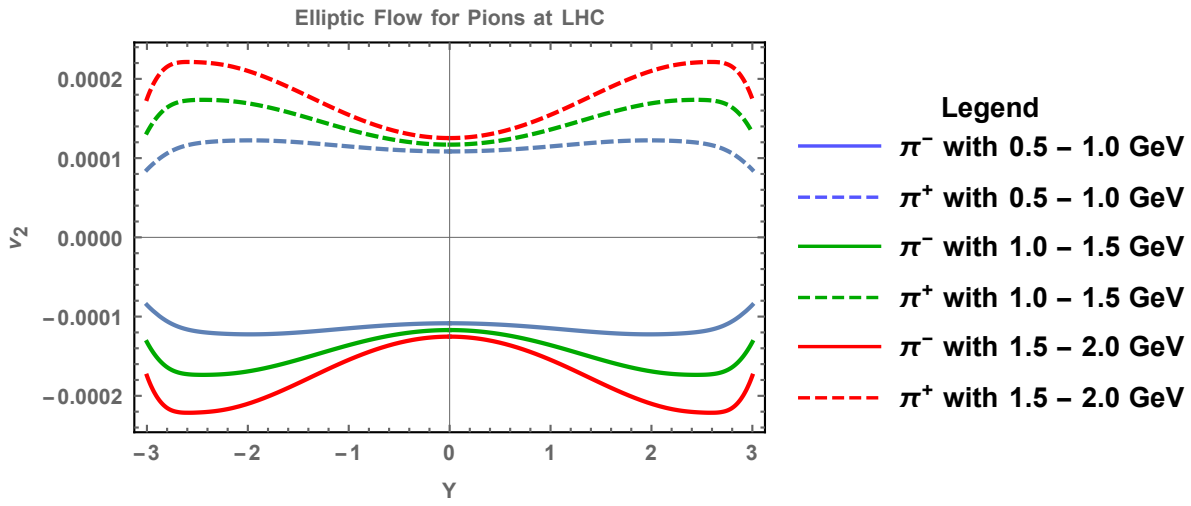

Figure 21: The elliptic flow at some larger transverse momentum bins for pions at LHC.

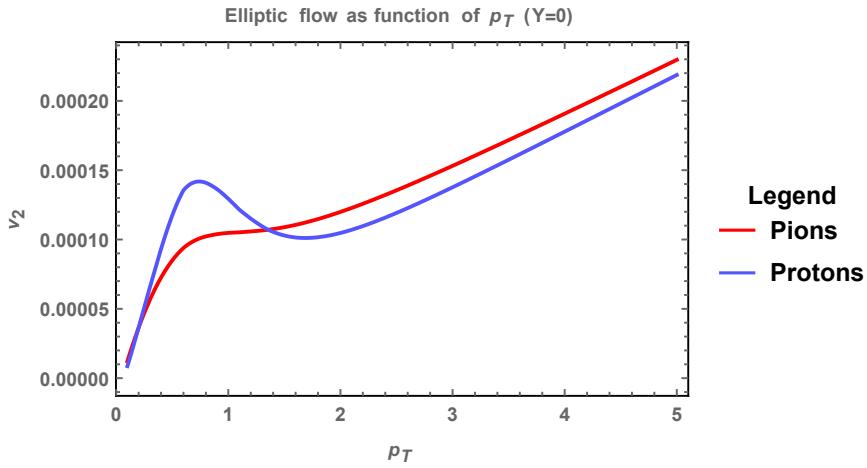

Figure 22: This plot shows the elliptic flow v_2 as a function of the transverse momentum. This is for pions and protons at mid rapidity $Y = 0$.

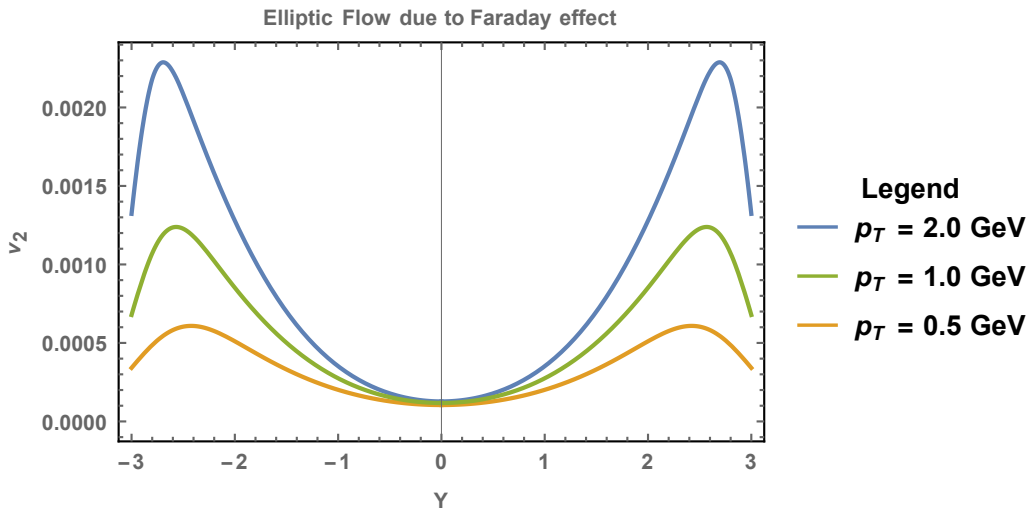

Figure 23: This plot shows the elliptic flow for positively charged pions due to only the Faraday effect. We show this for several values of the transverse momentum p_T. Note that the elliptic flow is in this case bigger than when we incorporate both magnetic effects, so again the Faraday and Hall effect are opposite of sign.

6.4 FARADAY AND HALL

Just as shown in the last section, we can again see the different contributions of the two magnetic effects. We show the results in Fig 23. The peculiar peaks that were visible in the v_2 plots at high p_T can thus be explained by a more pronounced peak in the Faraday effect.

6.5 TRIANGULAR FLOW v_3

Using the obtained recipe for v_n we have also generated results for the next harmonic. Note that we do again expect the rapidity asymmetry due to the symmetries present in our problem. See Fig 24.
If we compare the triangular flow to that found at the directed flow we see that these harmonics are almost identical in magnitude. A comparison for $p_T = 1.0$ GeV is shown in Fig 25.
We have also integrated the triangular flow from $p_T = 0.5$ GeV to 5.0 GeV, the results are shown in Fig 26

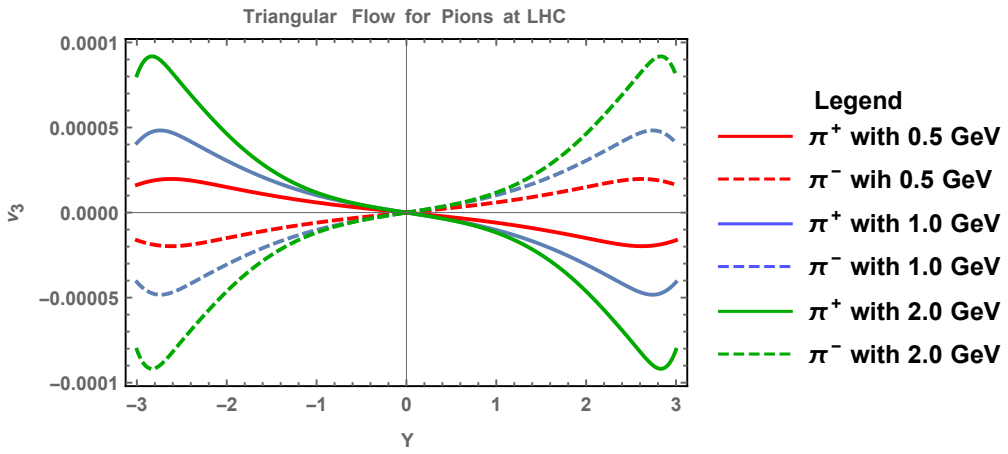

Figure 24: Here we show the triangular flow v_3 as function of the rapidity Y. Note that this (odd) harmonic has again the asymmetry in the rapidity.

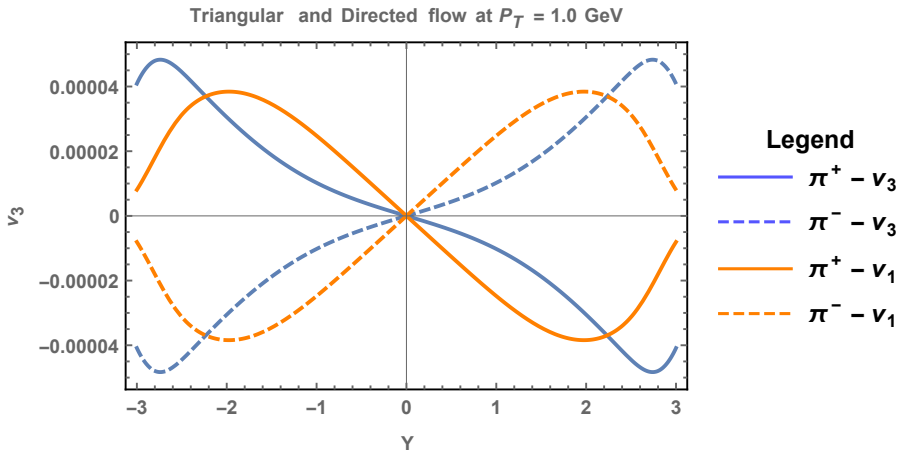

Figure 25: A comparison between the directed and the triangular flow. It is for pions at LHC where $p_T = 1$ GeV. Note that these harmonics are about equal in magnitude.

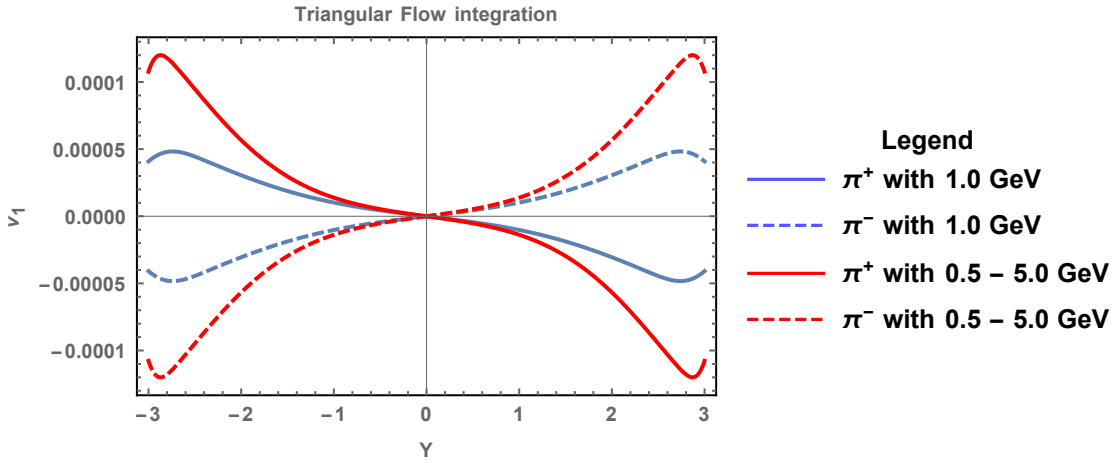

Figure 26: The triangular flow integrated from $p_T = 0.5$ GeV to 5.0 GeV. For comparison we included the triangular flow at pT = 1.0 GeV.

7 PARAMETER VARYING

7.1 INTRODUCTION

In this chapter we shall discuss the influence of the chosen parameters on the eventual result of the flow harmonics. The focus is mostly on the magnetic field, centrality (and impact parameter), conductivity and the drag force parameter. Note that we show mostly only the influence on either the B-field or the directed flow.

This chapter is included to provide information on how the result of flow harmonics can be influenced by varying the parameters. So that if a (slightly) different result is experimentally found we can always look at the influence of certain parameters on the outcome.

7.2 THE MAGNETIC FIELD

We also show how the directed flow is affected by changing the magnetic field by a certain factor α. The results are shown in Fig 27.
As we could have expected the relation is linear.

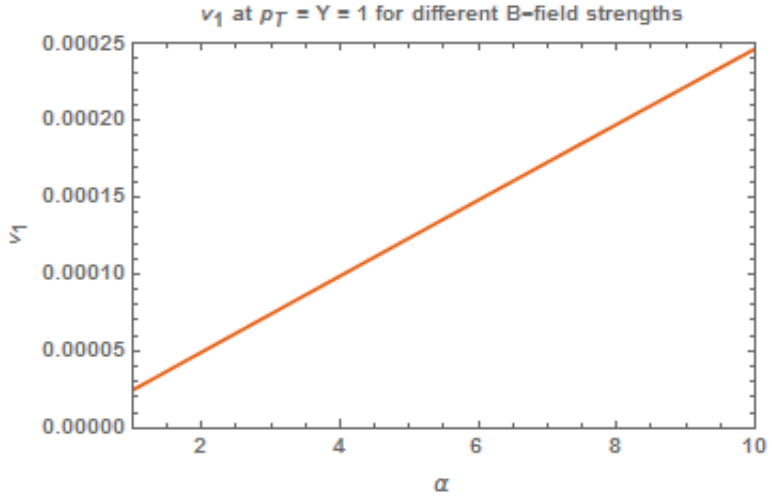

Figure 27: Here is shown the directed flow v_1 against the parameter α, which is the factor by which we increase the magnetic field ($\alpha\vec{B}$)

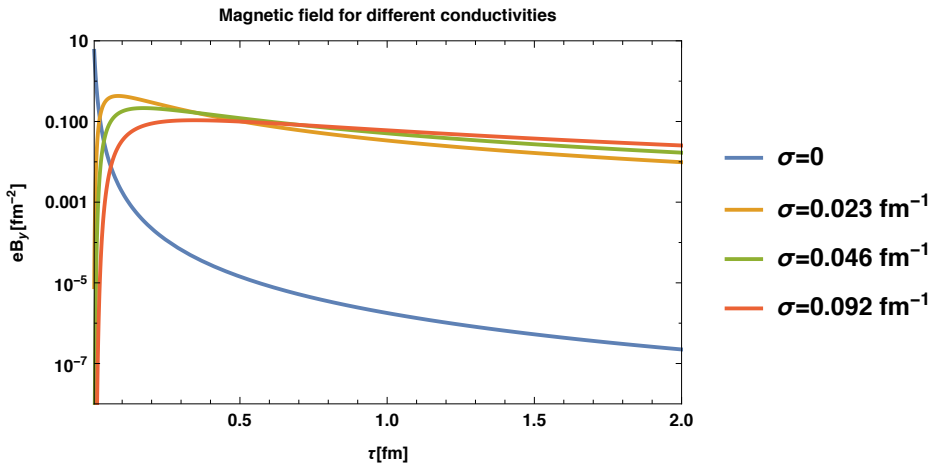

Figure 28: This plot shows the magnetic field ($\hat{y}$ direction) as a function of proper time τ, for different conductivities. In previous calculations we used the σ indicated by the yellow line ($0.023\ fm^{-1}$).

7.3 CONDUCTIVITY

The conductivity is a very important parameter, as it determines how fast the $\vec{B}$ field will decay. We show in Fig 28 the decay of the magnetic field for several values of this conductivity. In previous calculations we have used the value $\sigma = 0.023\ fm^{-1}$

Apart from the influence on the B-field itself it is also important to see the eventual outcome on the flow harmonics. In order to obtain minimum and maximum values of the conductivity we use ref [27] for recent lattice calculations.

The results are conventionally quoted as $C_{em}^{-1}\sigma/T$. We use that $C_{em} = (\frac{4}{9} + \frac{1}{9} + \frac{1}{9})e^2 = 0.061$ for 3-flavour QCD and thus 0.051 for 2-flavour QCD, to obtain both a minimum and maximum for σ.
We approximate the $T_{min} \approx 200$ MeV and $T_{max} \approx 600$ MeV.

Now using the results of [27] we approximate that $\sigma_{min} \simeq 0.0052 fm^{-1}$ and $\sigma_{max} \simeq 0.092 fm^{-1}$.
To obtain the influence on the directed flow we recalculate first the magnetic field with the appropriate conductivity. After this we can compute the directed flow for the different conductivities, shown in Fig 29.

7.4 IMPACT PARAMETER

In this section we explore the influence of the impact parameter on the B-field and the directed flow. Note that inherently the impact parameter is linked to the centrality and we will explore this in the next

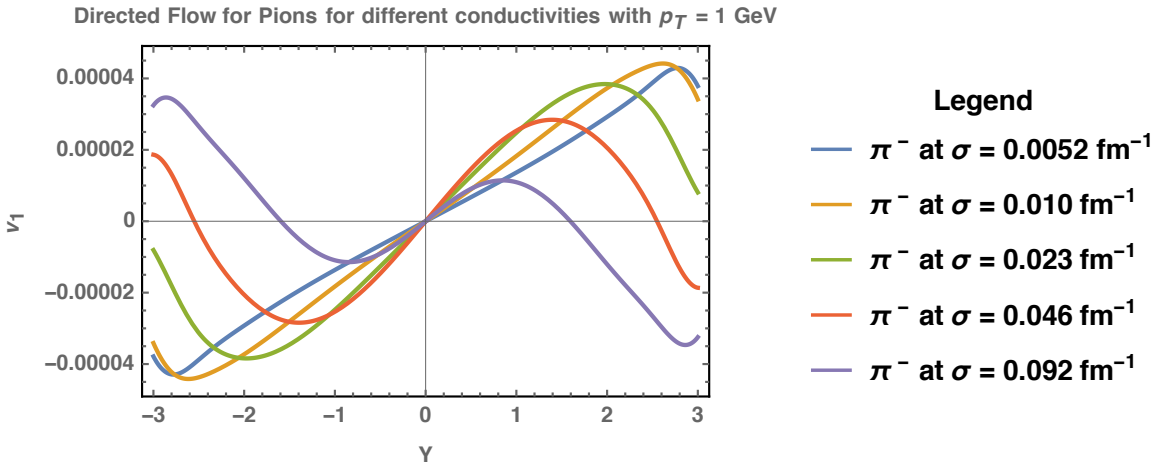

Figure 29: Here we show the directed flow for different centralities. Note that for clarity we only show negatively charged pions. The green line ($0.023 \mathrm{fm}^{-1}$) corresponds to earlier calculations.

section.
We however introduce this section, because according to ref. [28] perhaps a value of $b = 7.8$ fm is more realistic than our 7 fm.

First we show the magnetic field in the $\hat{y}$ direction (eB_y) as a function of the impact parameter, Fig 30.

Next we look at the influence of b on the directed flow itself, see Fig 31 and Fig 32. Note that as we increase the impact parameter the magnetic field produced by spectators increases, as the collision becomes more peripheral. This has also as a direct consequence that the directed flow increases.

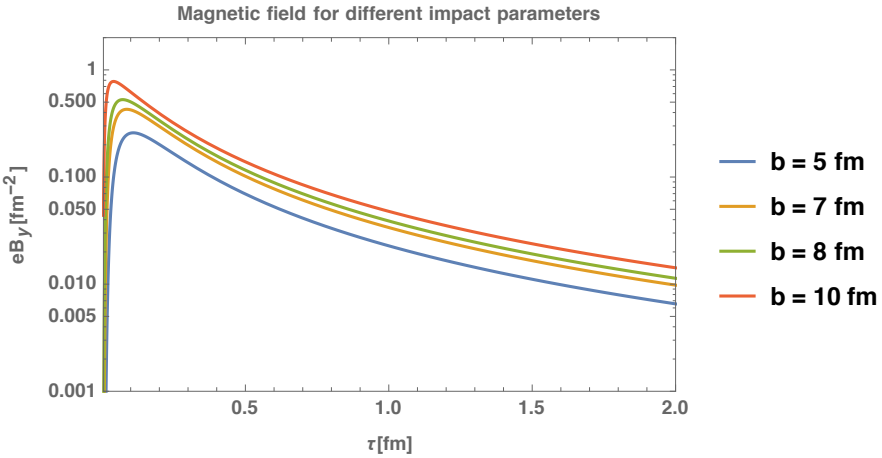

Figure 30: This plot shows the magnetic field ($\hat{y}$ direction) as a function of proper time τ, for different impact parameters. For reference, in previous chapters we used $b = 7$ fm. Note that this is a logarithmic plot.

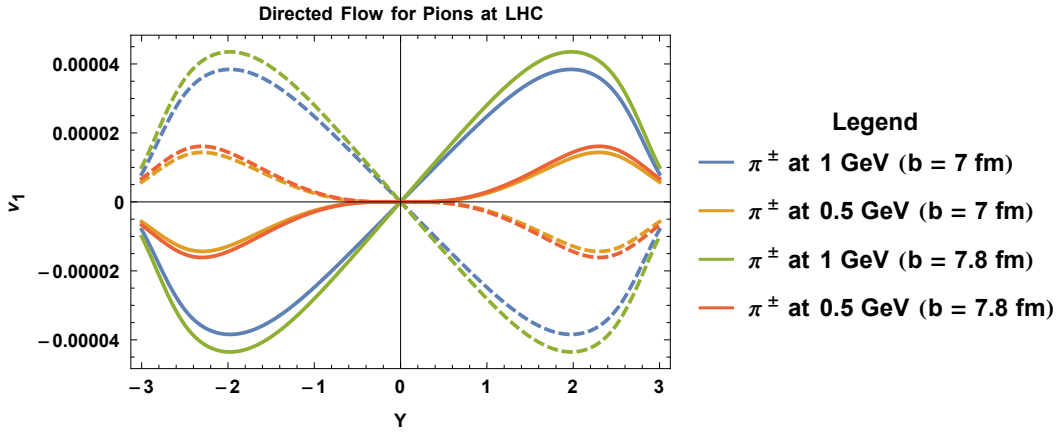

Figure 31: Here we show the directed flow for pions at p_T is 0.5 or 1 GeV, for b is either 7 or 7.8.

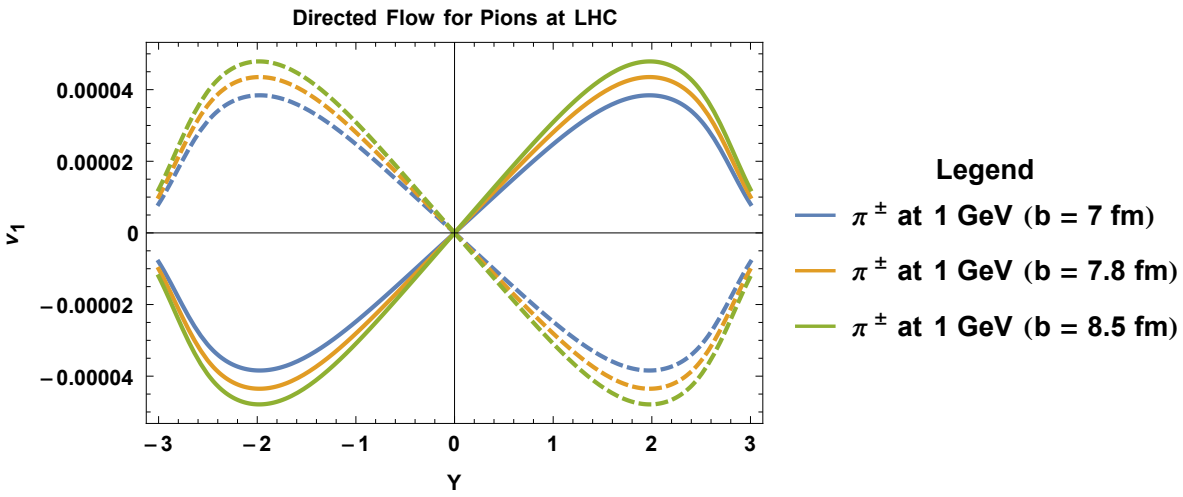

Figure 32: This plot shows the directed flow for different values of the impact parameter. Increasing impact parameter leads to a bigger directed flow.

7.5 CENTRALITY AND IMPACT PARAMETER

To determine the influence of centrality on the directed flow we must first recalculate v_0, Gubser's flow. For each centrality we obtain the necessary data from the ALICE collaboration [22], and pick the parameters q and T0 to obtain the best fit.

In Chapter 4 we showed in Fig 10 the obtained spectra for 20-30 % centrality and found the best fit parameters $q^{-1} = 6.4$ fm and $T_0 = 10.8$. We do now the same for 0-5, 5-10, 10-20 and 30-40 % centrality, shown in Fig 33, Fig 34, Fig 35 and Fig 36 respectively.

And also for every centrality we must recalculate the B-field using an appropriate impact parameter. Using again ref [28] we use the following values

$$0-5\% \rightarrow b = 1.75 \text{ fm}$$
$$5-10\% \rightarrow b = 4.3 \text{ fm}$$
$$10-20\% \rightarrow b = 6.0 \text{ fm}$$
$$20-30\% \rightarrow b = 7.8 \text{ fm}$$
$$30-40\% \rightarrow b = 9.2 \text{ fm}$$

After having obtained the respective v_0's and appropriate B-fields we can determine the directed flow, shown in Fig 37.
As one can see, a higher centrality yields a higher directed flow. This is expected due to the fact that a more peripheral collision yields more spectators and thus a bigger flow.

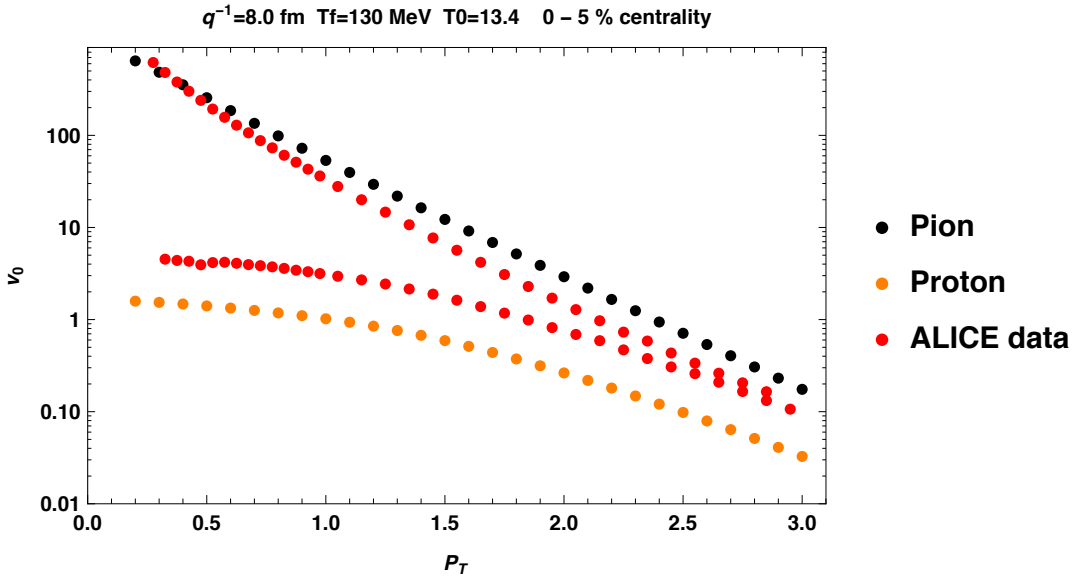

Figure 33: This plot shows the v_0 that originates from Gubser's flow for $0-5\%$. Our best fit parameters were $q^{-1} = 8.0$ fm and $T0 = 13.4$. This corresponds to $T = 660$ MeV for $\tau = 0.6$ fm at the center of the collision and an average temperature within $x_\perp < 7$ fm at $\tau = 0.6$ fm of 574 MeV.

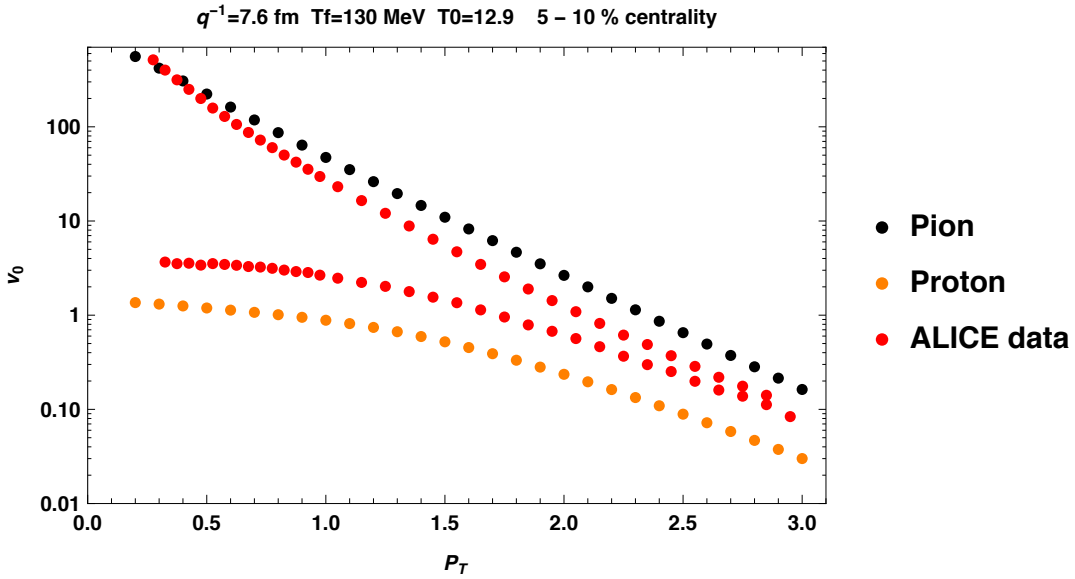

Figure 34: This plot shows the v_0 that originates from Gubser's flow for $5-10\%$. Our best fit parameters were $q^{-1} = 7.6$ fm and $T0 = 12.9$. This corresponds to $T = 657$ MeV for $\tau = 0.6$ fm at the center of the collision and an average temperature within $x_\perp < 7$ fm at $\tau = 0.6$ fm of 565 MeV.

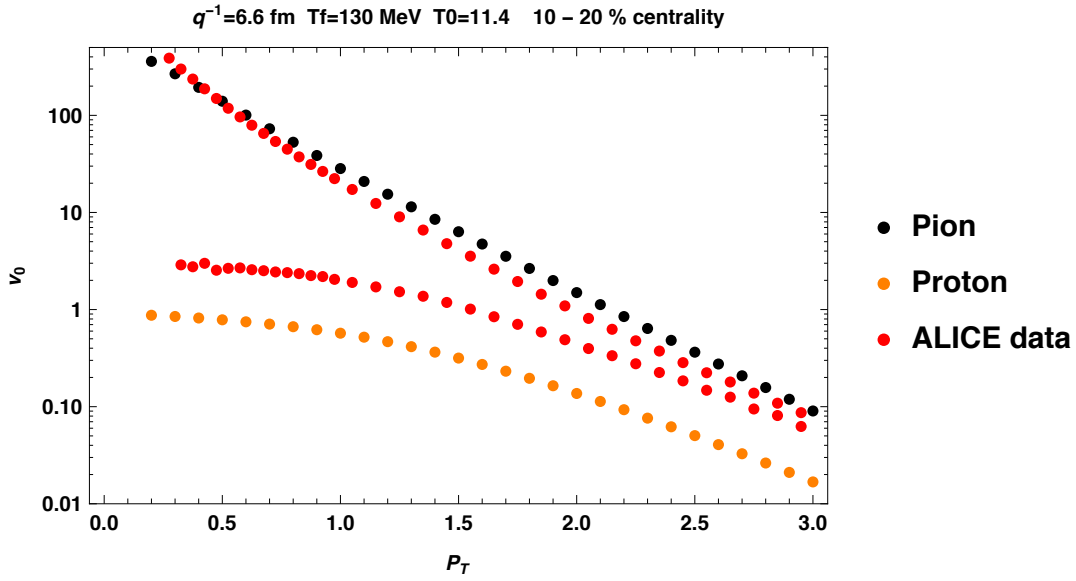

Figure 35: This plot shows the v_0 that originates from Gubser's flow for $10-20\%$. Our best fit parameters were $q^{-1} = 6.6$ fm and $T0 = 11.4$. This corresponds to $T = 638$ MeV for $\tau = 0.6$ fm at the center of the collision and an average temperature within $x_\perp < 7$ fm at $\tau = 0.6$ fm of 528 MeV.

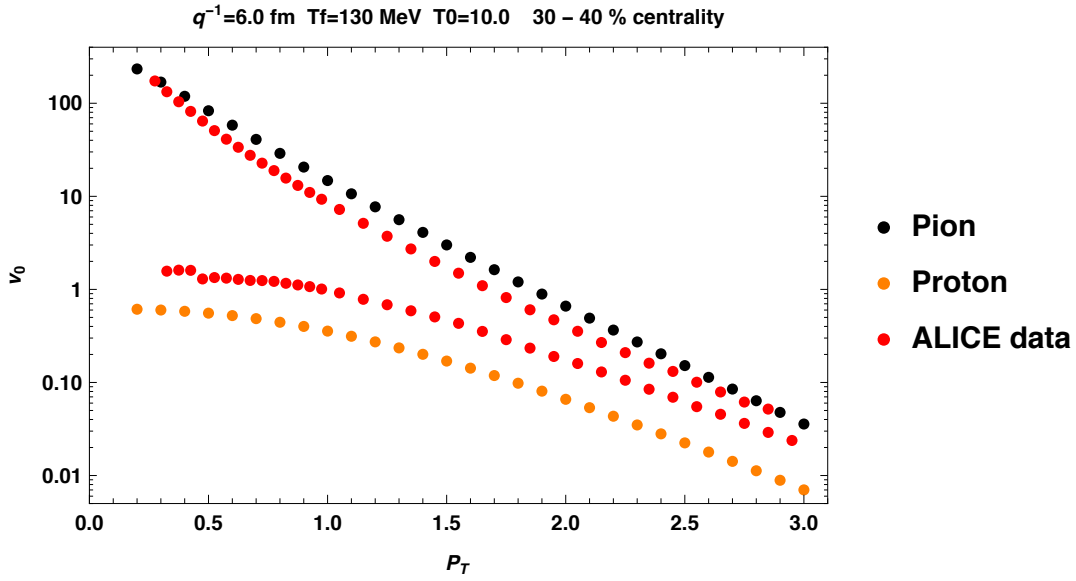

Figure 36: This plot shows the v_0 that originates from Gubser's flow for $30-40\%$. Our best fit parameters were $q^{-1} = 6.0$ fm and $T0 = 10.0$. This corresponds to $T = 595$ MeV for $\tau = 0.6$ fm at the center of the collision and an average temperature within $x_\perp < 7$ fm at $\tau = 0.6$ fm of 479 MeV.

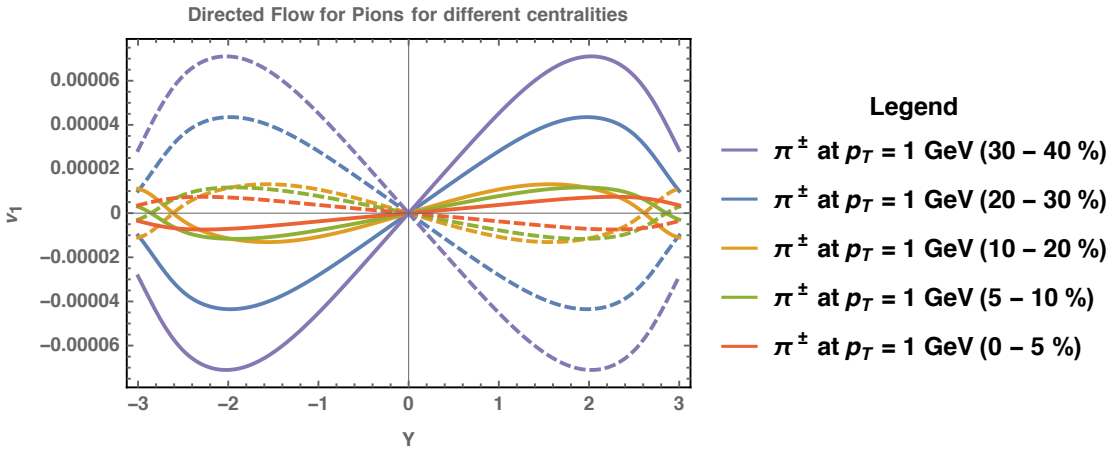

Figure 37: Here we show the directed flow (pions) for the different centralities.

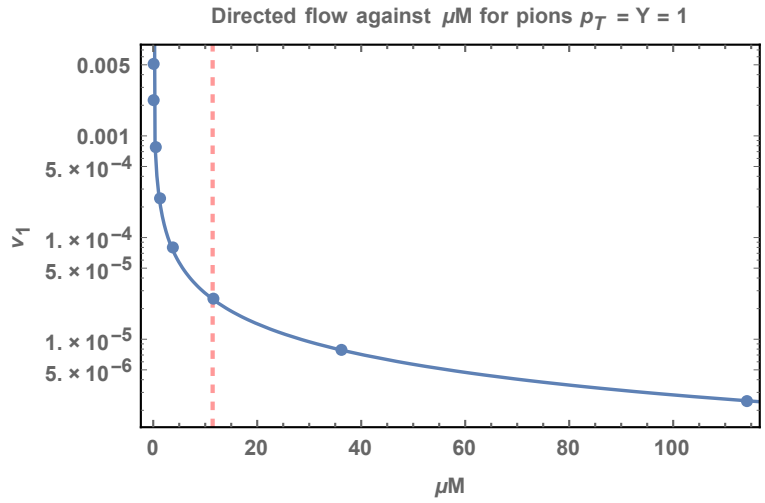

Figure 38: Here we show the directed flow v_1 against the drag force coefficient μm. Note that $v_1 \propto \frac{1}{\mu m}$. The red dashed curve indicates the value we used in previous chapters.

7.6 DRAG FORCE

In this last section we will look at probably the most important parameter, the drag force coefficient. In order to find our velocity (in the fluid rest frame) due to the electromagnetic fields we use, as showed in Equation 5, the following expression.

$$m \frac{d\vec{v}'}{dt} = q\vec{E}' + q\vec{v}' \times \vec{B}' - \mu m \vec{v}' = 0 \tag{94}$$

We now obtain the directed flow v_1 as a function of this coefficient μm. The results are shown in Fig 38. In this particular plot we look at the case $p_T = Y = 1$ for pions.

8

CONCLUSIONS AND A LOOK AHEAD

8.1 ELECTROMAGNETIC FIELDS AND ANISOTROPIC FLOW

Our motivation for this study was to figure out the influence of electromagnetic fields on the expansion of the QGP. Finding this influence means that we want to find out the influence on the different flow harmonics of the expansion.
As it turns out, the electromagnetic fields result in charge-dependent contributions to the flow components. In our case we obtained results for the directed flow (v_1), elliptic flow (v_2) and the triangular flow (v_3).

8.1.1 *Directed flow*

Results of v_1 are shown in Chapter 5 and in particular in Fig 11 till Fig 16. The most notable conclusions here are:

- The effect is small (around 0.0001) compared to the background v_1 that is present in HIC, which is of order 0.1.
- It is a charge dependent effect and thus neutral particles are unaffected.
- This charge dependent directed flow is also asymmetric in rapidity.

8.1.2 *Elliptic flow*

In Chapter 6 and Fig 18 till Fig 21 the results for v_2 are shown.

- The found elliptic flow is about one order of magnitude bigger than the directed flow.
- It is symmetric in rapidity, unlike the directed flow and triangular flow.

8.1.3 *Triangular flow*

In Chapter 6 and in particular in Fig 24 till Fig 26 the results for v_3 are shown.

- The charge dependent triangular flow is about the same order of magnitude as the directed flow.
- Just as v_1, it is also asymmetric in rapidity.

8.2 PARAMETER STUDY

In Chapter 7 we studied several important variables of our calculations. From these calculations it is apparent that especially the centrality and the drag force parameter are important.

The centrality affects the eventual charge dependent v_1 quite heavily, Fig 37. These results are not that surprising since increasing the centrality makes the collisions more peripheral which in turn results in more spectator particles. These spectators are the biggest contributor to the electromagnetic fields and thus we expect a larger v_1.

The drag force parameter has a relation to the produced v_1 as $v_1 \propto \frac{1}{\mu m}$, Fig 38. This is therefore the most sensitive parameter and quite possibly the first one to be looked at in the case of an experimental mismatch.

8.3 A LOOK AHEAD

In our efforts to maintain an analytic solution we made several assumptions that may have some influence on the obtained end results. The QGP is of course a dynamic system, a more realistic situation would be created with adjusting the following adjustments.

- A time (or temperature) dependent conductivity σ.
- A dynamic drag force coefficient μ_m.
- Including realistic particle densities for the u and d (anti)quarks.
- Including other quark types (strange, charm etc).
- A chemical potential due to baryon number or isospin.

Apart from the above adjustments to several parameters, we also argue for the importance of a complete numerical hydrodynamic model. This numerical model would then include realistic background flow harmonics, which the analytic model by Gubser lacks. A proper candidate is perhaps VISH2+1 [29]. This model assumes boost invariance and solves the hydrodynamic equations in order to obtain the flow field u^μ and local temperature.

Another interesting addition could be the Chiral Magnetic Effect [30] [31]. This effect could result in a contribution to the magnetic fields and would be included also in the equation of motion.

Part II

APPENDIX

The appendix will deal with a few of the methods we used to obtain our results. We show here how we approximated the electromagnetic field, the calculation of the directed flow and a small discussion on integration over transverse momentum.

APPENDIX I

In this appendix we shall discuss the numerical integration. To start, we have used Mathematica (9 or 10) to obtain every result.
Although Mathematica has many good points, usually computational efficiency is not one of these. We tried however to get the best efficiency possible by using a mostly multi-core approach.

A.1 NUMERICAL INTEGRATION EXAMPLES

A.1.1 *B-field*

In order to obtain the B-field for values of η, $x_\perp$ and ϕ we created a large of numerical integrations of the expressions Equation 51 and Equation 52. This was done by evaluating these expressions at a large multitude of values for η, $x_\perp$ and ϕ and thereby creating a large table, see also Listing 1.

The most important features are the including of the command Parallelize and Multiperiodic. The first of these (as the name suggests) parallelizes the table over all available cores. The second is a certain method for solving the numerical integrations.
Without these enabled the calculation would take about 4-5 hours to complete, while now it takes a mere 10 minutes (quad-core). The final step we made was an interpolation of this table to use in our final result for the B-field.

A.1.2 *Flow calculations and pT distributions*

The flow calculations were obtained also by approximating the integrals with summations. First we use the calculation of v_1 as shown in Listing 2 and continued in Listing 3. As an example of the approximate integral, a directed flow calculation is shown in Listing 4.

Listing 1: B field approximation

```
ItabE = Parallelize[
  Table[{{\[Eta],
      xp1, \[Phi]} = {-3 +
       6 (n - 1)/points, .001 + (m - 1) (xpf - 0.001)/
        points, -\[Pi] + (k - 1) 2 \[Pi]/
         points}; \[Tau] = \[Tau]freeze[xp1]; NIntegrate[Clear[
             Int];
         Int[\[Phi]p_?NumericQ] := (Int[\[Phi]p] =
       NIntegrate[
       Sqrt[RA^2 - x^2 + b x Cos[\[Phi]p] - b^2/4] x  Sinh[
         Y0] (\[Tau]^2 Sinh[Y0 - \[Eta]]^2 + xp^2 + x^2 -
           2 xp x Cos[\[Phi] - \[Phi]p])^(-3/2) (xp Cos[\[Phi]] -
          x Cos[\[Phi]p]) (\[Sigma] Sinh[
            Y0] Sqrt[\[Tau]^2 Sinh[Y0 - \[Eta]]^2 + xp^2 + x^2 -
              2 xp x Cos[\[Phi] - \[Phi]p]]/2 +
          1) Exp[\[Sigma] Sinh[Y0 - \[Eta]] Sinh[Y0] \[Tau]/
            2 - \[Sigma]/2 Sinh[
            Y0] Sqrt[\[Tau]^2 Sinh[Y0 - \[Eta]]^2 + xp^2 + x^2 -
             2 xp x Cos[\[Phi] - \[Phi]p]]], {x, -Cos[\[Phi]p] b
                 /2 +
         Sqrt[RA^2 - b^2 Sin[\[Phi]p]^2/4],
        Cos[\[Phi]p] b/2 + Sqrt[RA^2 - b^2 Sin[\[Phi]p]^2/4]}]);
   Int[\[Phi]p], {\[Phi]p, -\[Pi]/2, \[Pi]/2}]}, {n, 1,
  points + 1}, {m, 1, points + 1}, {k, 1, points + 1}]]
```

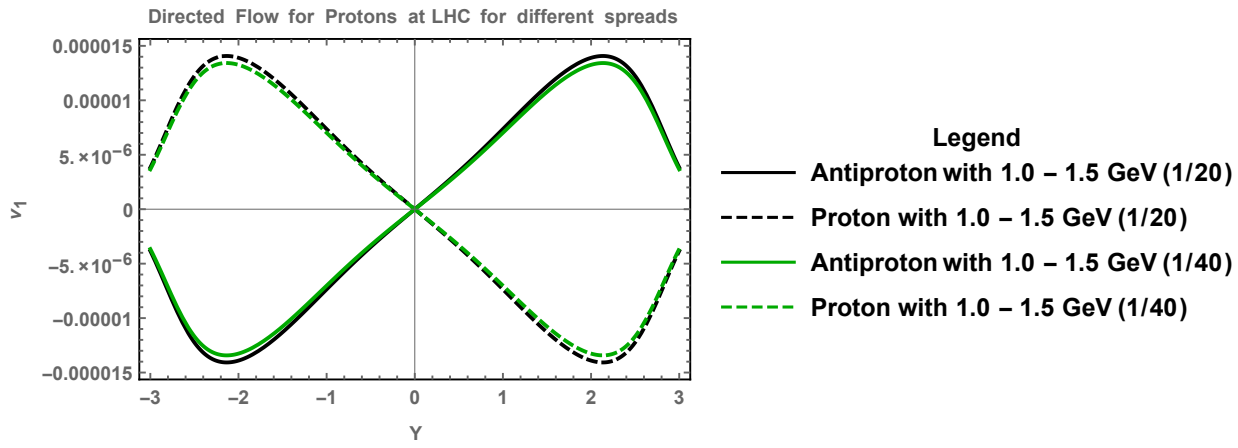

Figure 39: Here we compare the directed flow for p_T from 1.0 to 1.5 GeV for different bin sizes. As can be seen, the difference between the two is minimal.

In the listing, vcomputesTot; v1el contains the calculation to the directed flow itself and as can be seen, the total directed flow follows from a summation of all the values.

To now integrate this over a p_T distribution, for example from 1 to 1.5 GeV, one has to do this calculation in Listing 4 for several values of p_T and add these up. The key here is to find the right bin-size to use between two consecutive of p_T. We found that a bin-size of $\frac{1}{20}$ obtained results precise enough for a order of magnitude estimate. See also Fig 39.

Listing 2: Directed flow

```
vcomputesTot := (\[Tau] = \[Tau]freeze[xp]; \[Tau]p = \[Tau]
    freeze'[
    xp]; \[Kappa] =
   ArcTanh[2 q^2 \[Tau] xp/(1 + q^2 \[Tau]^2 + q^2 xp^2)];
  By = -Z 3 e /(8 \[Pi]^2 RA^3) (Bfield[\[Eta], xp,
       Mod[\[Pi] - \[Phi], 2 \[Pi], -\[Pi]]] +
      Bfield[-\[Eta], xp, \[Phi]]);
  Ex = Z 3 e /(8 \[Pi]^2 RA^3) (-Coth[Y0] Bfield[\[Eta], xp,
        Mod[\[Pi] - \[Phi], 2 \[Pi], -\[Pi]]] +
      Coth[Y0] Bfield[-\[Eta],
        xp, \[Phi]]);
  F = ({ {0, Ex, 0, 0},{-Ex, 0, 0, -By},{-0, 0, 0, 0},{-0, By, 0,
       0} });
  \[CapitalLambda]x = ({
      {\[Gamma], -\[Gamma] ux, -\[Gamma] uy, -\[Gamma] uz},
      {-\[Gamma] ux, 1 + ux^2 (\[Gamma] - 1)/u2,
       ux uy (\[Gamma] - 1)/u2, ux uz (\[Gamma] - 1)/u2},
      {-\[Gamma] uy, ux uy (\[Gamma] - 1)/u2,
       1 + uy^2 (\[Gamma] - 1)/u2, uz uy (\[Gamma] - 1)/u2},
      {-\[Gamma] uz, ux uz (\[Gamma] - 1)/u2, uz uy (\[Gamma] -
          1)/u2,
        1 + uz^2 (\[Gamma] - 1)/u2}
     }) /. {\[Gamma] -> Cosh[\[Eta]] Cosh[\[Kappa]],
     ux -> Cos[\[Phi]] Tanh[\[Kappa]]/Cosh[\[Eta]],
     uy -> Sin[\[Phi]] Tanh[\[Kappa]]/Cosh[\[Eta]],
     uz -> Tanh[\[Eta]],
     u2 -> (Tanh[\[Kappa]]^2 + Sinh[\[Eta]]^2)/Cosh[\[Eta]]^2};
  Fp = \[CapitalLambda]x.F.\[CapitalLambda]x;
  Epx = Fp[[1, 2]]; Epy = Fp[[1, 3]]; Epz = Fp[[1, 4]];
  Bpx = Fp[[3, 4]]; Bpy = -Fp[[2, 4]]; Bpz = Fp[[2, 3]];
  Mdb = {{-\[Mu]M, e/3 Bpz, -e/3 Bpy}, {-e/3 Bpz, -\[Mu]M,
     e/3 Bpx}, {e/3 Bpy, -e/3 Bpx, -\[Mu]M}};
  vdb = Inverse[Mdb].{-e/3 Epx, -e/3 Epy, -e/3 Epz};
  Mu = {{-\[Mu]M, 2 e/3 Bpz, -2 e/3 Bpy}, {-2 e/3 Bpz, -\[Mu]M,
     2 e/3 Bpx}, {2 e/3 Bpy, -2 e/3 Bpx, -\[Mu]M}};
  vu = Inverse[Mu].{-2 e/3 Epx, -2 e/3 Epy, -2 e/3 Epz};
```

Listing 3: Directed flow - continued

```
vp = (vu + vdb)/2;
 \[Gamma]p = 1/Sqrt[1 - vp[[1]]^2 - vp[[2]]^2 - vp[[3]]^2];
 \[CapitalLambda]px = ({
     {\[Gamma], \[Gamma] ux, \[Gamma] uy, \[Gamma] uz},
     {\[Gamma] ux, 1 + ux^2 (\[Gamma] - 1)/u2,
      ux uy (\[Gamma] - 1)/u2, ux uz (\[Gamma] - 1)/u2},
     {\[Gamma] uy, ux uy (\[Gamma] - 1)/u2,
      1 + uy^2 (\[Gamma] - 1)/u2, uz uy (\[Gamma] - 1)/u2},
     {\[Gamma] uz, ux uz (\[Gamma] - 1)/u2, uz uy (\[Gamma] - 1)
         /u2,
      1 + uz^2 (\[Gamma] - 1)/u2}
    }) /. {\[Gamma] -> Cosh[\[Eta]] Cosh[\[Kappa]],
    ux -> Cos[\[Phi]] Tanh[\[Kappa]]/Cosh[\[Eta]],
    uy -> Sin[\[Phi]] Tanh[\[Kappa]]/Cosh[\[Eta]],
    uz -> Tanh[\[Eta]],
    u2 -> (Tanh[\[Kappa]]^2 + Sinh[\[Eta]]^2)/Cosh[\[Eta]]^2};
 v = \[CapitalLambda]px.Flatten[{\[Gamma]p, \[Gamma]p vp}];
 TR = {{Cosh[\[Eta]], 0, 0, -Sinh[\[Eta]]}, {0, Cos[\[Phi]],
    Sin[\[Phi]], 0}, {-Sinh[\[Eta]]/\[Tau], 0, 0,
    Cosh[\[Eta]]/\[Tau]}, {0, -Sin[\[Phi]]/xp, Cos[\[Phi]]/xp,
        0}};
 vB = TR.v;
 v\[Tau]totfreez = vB[[1]];
 vptotfreez = vB[[2]];
 v\[Eta]totfreez = vB[[3]];
 v\[Phi]totfreez = vB[[4]];
 W = vptotfreez^2 + (xp v\[Phi]totfreez)^2;
 mT\[Pi] = Sqrt[(pT)^2 + (m\[Pi])^2];
 v1el = \[Tau] xp Exp[-(mT\[Pi]/Tff) Cosh[
       Y - \[Eta]] v\[Tau]totfreez + \[Tau] (mT\[Pi]/Tff) Sinh[
       Y - \[Eta]] v\[Eta]totfreez] ((vptotfreez Cos[\[Phi]] -
        xp v\[Phi]totfreez Sin[\[Phi]]) (mT\[Pi] Cosh[
          Y - \[Eta]] BesselI[1, (pT/Tff) Sqrt[W]]/
          Sqrt[W] - \[Tau]p pT vptotfreez/
          W (BesselI[0, (pT/Tff) Sqrt[W]] -
           Hypergeometric0F1[2, (pT/Tff)^2 1/4 W])) - \[Tau]p pT
              /
       2 Cos[\[Phi]] Hypergeometric0F1[2, (pT/Tff)^2 1/4 W] ))
```

Listing 4: Directed flow final calculation

```
Do[{Unset[tab], Y = -3 + 0.1 i,
   tab =
    Parallelize[
     Table[{\[Eta], xp, \[Phi], vcomputesTot; v1el}, {\[Eta], -3,
          3,
       6/points}, {xp, 0.001, xpf - (xpf - 0.001)/points, (
       xpf - 0.001)/points}, {\[Phi], -\[Pi], \[Pi] - 2 \[Pi]/
           points,
       2 \[Pi]/points}]],
   v1 = Total[Flatten[tab, 2][[1 ;; -1, 4]]] (xpf - 0.001)/
     points (6/points) 2 \[Pi]/
      points 2 (0.197)^(-3) (2 \[Pi])^(-2)/(2 \[Pi] v0\[Pi][2, pT
          , 1/
        6.4]),
   AppendTo[PionPT1v1, {Y, Re[v1]}], Print[{Y, Re[v1]}]}, {i, 0,
      30}];
```

[1] Umut Gürsoy et al., Magnetohydrodynamics, charged current and directed flow in heavy ion collisions. Phys. Rev. C 89, 054905 (2014)

[2] K. Tuchin, Adv. High Energy Phys. 2013, 490495 (2013) [arXiv:1301.0099]

[3] T. Lappi and L. McLerran, Nucl. PHys. A 772, 200 (2006) [hep-ph/0602189]

[4] J. -P. Blaizot, F. Gelis, J. Liao, L. McLerran and R. Venugopalan, arXiv:1210.6838 [hep-ph]

[5] H.-T. Ding, A. Francis, O. Kaczmarek, F. Karsch, E. Laermann and W.Soeldner, Phys. Rev. D 83, 034504 (2011) [arXiv:1012.4963 [hep-lat]]

[6] A. Francis and O. Kaczmarek, Prog. Part. Nucl. Phys. 67, 212 (2012) [arXiv:1112.4802 [hep-lat]]

[7] B. B. Brandt, A. Francis, H. B. Meyer and H. Wittig, JHEP 1303, 100 (2013) [arXiv:1212.4200 [hep-lat]]

[8] A. Amato, G. Aarts, C. Allton, P. Giudice, S. Hands and J. -I. Skullerud, Phys. Rev. Lett. 111, 172001 (2013) [arXiv:1307.6763 [hep-lat]]

[9] O. Kaczmarek and M. Mller, arXiv:1312.5609 [hep-lat]

[10] Gradshteyn Ryzhik Table of Integrals, Series and Products

[11] D. E. Kharzeev, L. D. McLerran and H. J. Warringa, Nucl. Phys. A 803, 227 (2008) [arXiv:0711.0950]

[12] D. Kharzeev, Phys. Lett. B 378, 238 (1996) [nucl-th/9602027]

[13] E. Abbas et al. [ALICE Collaboration], Eur. Phys. J. C 73, 2496 (2013) [arXiv:1305.1562 [nucl-ex]]

[14] S. S. Gubser, Phys. Rev. D 82, 085027 (2010) [arXiv:1006.0006 [hep-th]].

[15] S. Borsanyi, G. Endrodi, Z. Fodor, A. Jakovac, S. D. Katz, S. Krieg, C. Ratti and K. K. Szabo, JHEP 1011, 077 (2010) [arXiv:1007.2580 [hep-lat]].

[16] H. B. Meyer, Phys. Rev. D 76, 101701 (2007) [arXiv:0704.1801 [hep-lat]].

[17] G. Policastro, D. T. Son, and A. O. Starinets, "The shear viscosity of strongly coupled N = 4 supersymmetric Yang-Mills plasma," Phys. Rev. Lett. 87 (2001) 081601, [hep-th/0104066].

[18] P. Kovtun, D. T. Son, and A. O. Starinets, "Viscosity in strongly interacting quantum field theories from black hole physics," Phys. Rev. Lett. 94 (2005) 111601, [hep-th/0405231].

[19] C. Shen and U. Heinz, Phys. Rev. C 85, 054902 (2012) [Erratum-ibid. C 86, 049903 (2012)] [arXiv 1202.6620 [nucl-th]].

[20] F. Cooper and G. Frye, Phys. Rev. D 10, 186 (1974).

[21] P. Romatschke "New developments in relativistic viscous hydrodynamics" Int.J.Mod.Phys.E19:1-53,2010 arXiv:0902.3663 [hep-ph]

[22] B. Abelev et al. [ALICE Collaboration], Phys. Rev. C 88, 044910 (2013) [arXiv:1303.0737 [hep-ex]].

[23] R. Snellings, "Elliptic flow: a brief review," New Journal of Physics, vol. 13, Article ID 055008, 2011.

[24] C. P. Herzog, A. Karch, P. Kovtun, C. Kozcaz and L. G. Yaffe, JHEP 0607, 013 (2006) [hep-th/0605158].

[25] J. Casalderrey-Solana and D. Teaney, Phys. Rev. D 74, 085012 (2006) [hep-ph/0605199].

[26] S. S. Gubser, Phys. Rev. D 74, 126005 (2006) [hep-th/0605182].

[27] - A. Amato, G. Aarts, C. Allton, P. Giudice, S. Hands and J. -I. Skullerud, Phys. Rev. Lett. 111, 172001 (2013) [arXiv:1307.6763 [hep-lat]].

[28] - ALICE Collaboration, Centrality determination of Pb-Pb collisions at $\sqrt{s_{NN}} = 2.76$ TeV with ALICE. Phys. Rev. C 88 (2013) 044909 [arXiv:1301.4361]

[29] - H. Song and U. W. Heinz, Phys.Lett. B658, 279 (2008), arXiv:0709.0742 [nucl-th]; Phys.Rev. C77, 064901 (2008), arXiv:0712.3715 [nucl-th]; C78, 024902 (2008), arXiv:0805.1756 [nucl-th].

[30] - D. Kharzeev, L. McLerran, H. Warringa, Nucl.Phys.A803:227-253,2008, arXiv:0711.0950 [hep-ph]

[31] - K. Fukushima, D. Kharzeev, H. Warringa, Phys.Rev.D78:074033,2008, arXiv:0808.3382 [hep-ph]

COLOPHON

My thesis was typeset using the typographical look-and-feel `classicthesis` developed by André Miede. The style was inspired by Robert Bringhurst's seminal book on typography "*The Elements of Typographic Style*". `classicthesis` is available for both LaTeX and LyX:

`http://code.google.com/p/classicthesis/`

Several adjustments were made to the style by myself aswell.

Final Version as of June 16, 2015 (Magnetohydrodynamics at HIC version 1.0)